Catalysis Science & Technology

Accepted Manuscript

This article can be cited before page numbers have been issued, to do this please use: M. M. Antunes, P. Neves, A. Fernandes, S. Lima, A. F. Silva, M. F. Ribeiro, C.M. Silva, M. Pillinger and A. A. Valente, *Catal. Sci. Technol.*, 2016, DOI: 10.1039/C6CY00223D.

ROYAL SOCIETY OF CHEMISTRY

www.rsc.org/catalysis

DOI: 10.1039/C6CY00223D

Catalysis Science & Technology

ARTICLE

Bulk and composite catalysts combining BEA topology and mesoporosity for the valorisation of furfural

Received 00th January 20xx,
Accepted 00th January 20xx

DOI: 10.1039/x0xx00000x

www.rsc.org/

Margarida M. Antunes,[a] Patrícia Neves,[a] Auguste Fernandes,[b] Sérgio Lima,[a] Andreia F. Silva,[a] Maria F. Ribeiro,[b] Carlos M. Silva,[a] Martyn Pillinger*[a] and Anabela A. Valente*[a]

The sustainable conversion of biomass and biomass-derived platform chemicals demands efficient catalytic processes for which modified versions of zeolites can be strategically important. The catalytic potential of bulk and composite catalysts which simultaneously feature zeolite crystallinity, mesoporosity and Zr- and Al-sites, were explored for the valorisation of furfural (Fur), industrially produced from hemicelluloses, via integrated reduction and acid reactions in alcohol media, to give useful bio-products (bioP), namely furanic ethers, levulinate esters and angelica lactones. Different synthetic strategies were used starting from zeolite microcrystals or nanocrystals. A composite consisting of nanocrystals of Zr,Al-Beta embedded in a mesoporous matrix is reported for the first time. In a different synthesis approach, a bulk mesoporous zeotype material was synthesized by post-synthesis alkaline/acid/impregnation treatments, and explored for the first time as a catalyst for a one-pot reduction/acid reaction system. Characterisation studies of morphology, structure, texture and nature of the Al- and Zr-sites (^{27}Al MAS NMR spectroscopy, FT-IR of adsorbed pyridine or deuterated acetonitrile) helped understand the influence of material properties on catalytic performances. These types of materials are active and stable catalysts for the integrated conversion of Fur to bioP.

1. Introduction

The use of vegetable biomass as a renewable source of chemical energy demands the development of sustainable conversion processes in which a key principle is the use of catalysts, preferably heterogeneous ones.[1-5] In the field of heterogeneous catalysis, zeolites and zeotypes are highly versatile crystalline microporous catalysts possessing various topologies, and can be furnished with different types of acid and/or metal active sites.[6] Since the beginning of this century, extensive research has been performed to modify the textural and morphological properties of zeolites in order to operate under kinetic regime with improved catalytic performances in reactions involving relatively bulky molecules. This is particularly important for the chemical valorisation of non-edible lignocellulosic biomass (mainly composed of lignin and carbohydrate polymers) and derived platform chemicals.[5,7-9] Synthetic strategies include the introduction of mesoporosity in pre-formed zeolites, and, on the other hand, the reduction of the crystallite sizes down to the nanometer scale.

Mesoporosity can be introduced in zeolites via post-synthesis alkaline treatments, allowing enhanced active sites accessibility.[10-17] The application of this approach for improving the catalytic performances of zeolites for lignocellulosic biomass conversion processes is quite recent, and mainly focused on three types of commercially available zeolites, namely, ZSM-5, faujasite Y and Beta. The catalytic applications include: pyrolysis of lignocellulosic biomass;[18] hydrolytic hydrogenation of cellulose to sugar alcohols;[19] hydrolysis of cellulose to 5-hydroxymethylfurfural (HMF);[20] dehydration of fructose to HMF;[21] conversion of xylose (derived from hemicelluloses) to levulinic acid (LA);[22,23] conversion of furfuryl alcohol (FA) to levulinate esters (LEs),[24] esterification of LA to LEs;[25,26] aqueous-phase isomerization of bio-based dihydroxyacetone to lactic acid;[27] conversion of eugenol (model substrate for lignin monomers) to hydrocarbons.[28] The mesoporous zeotypes can be further modified to meet specific requirements. For acid-catalysed reactions, the alkaline treatment is usually followed by conventional ion-exchange to introduce acid sites. Stefanidis *et al.*[29] reported improved catalytic performance in biomass pyrolysis for a mordenite-type material prepared via sequential alkaline (to introduce mesoporosity) and strong acid (dealumination) treatments. Recently, Dapsens *et al.*[30] reported superior catalytic performance in isomerisation reactions of bio-based chemicals, for a Sn-containing Beta type catalyst prepared via post-synthesis treatment in a Sn/alkaline solution, which simultaneously introduced Sn-sites and mesoporosity in the bulk of the zeolite precursor.

[a] *CICECO - Aveiro Institute of Materials, Department of Chemistry, University of Aveiro, Campus Universitário de Santiago, 3810-193 Aveiro, Portugal. E-mail: mpillinger (mpillinger@ua.pt), atav@ua.pt (A.A. Valente).b*
[b] *Institute for Biotechnology and Bioengineering, Centre for Biological and Chemical Engineering, Instituto Superior Técnico, Av. Rovisco Pais, 1049-001 Lisboa, Portugal.*

† Electronic Supplementary Information (ESI) available: Catalysts characterisation results (PXRD, SEM, TEM, DR UV-vis, TGA, DSC) and catalytic results (influence of reaction conditions, type of alcohol, catalyst reuse for LA conversion, catalytic performance of synthesis precursors). See DOI: 10.1039/x0xx00000x

View Article Online
DOI: 10.1039/C6CY00223D

In a different approach, the crystallite sizes of zeolites can be reduced down to the nanometer scale, which is accompanied by enhanced surface area/micropore volume ratios, leading to reduced intracrystalline diffusional pathways, avoiding mass transfer limitations and extensive coke formation.[31-35] Nevertheless, concerns about the health and environmental effects of using nanoparticles[36], and technical issues (e.g. high pressure drops, clogging of equipments), place demands on the development of effective nano-catalyst formulations. In this sense, nanocrystalline zeolites (powder form or in suspension) have been blended into the synthesis mixtures of inorganic mesoporous phases possessing different pore arrangements, relatively narrow pore size distributions and high specific surface areas.[37-43] This approach is interesting for preparing catalyst formulations in which the mesoporous phase acts as an inorganic binder of nanocrystallites, provides a somewhat regular network of mesoporous channels for facilitated mass transport of reagents/products and active sites accessibility. This approach has been used to prepare composites of several zeolites (Beta,[38,40,42,44-53] Y,[54-56] L,[57-59] A,[60,61], ZSM-5[34,35,39,48,62-68], MCM-22[69]) or zeotypes (SAPO-5,[70,71] silicalite-1[72]) embedded in mesoporous siliceous phases. The structure of the mesoporous component depends partly on the type and concentration of the templating agent used: e.g. alkyl trimethyl ammonium bromide surfactants (C_nTAB, n=10, 12, 14 and 16) for MCM-41 type matrix possessing a one-dimensional (1D) hexagonal arrangement of cylindrical pores,[70,71] or MCM-48 possessing a 3D cubic pore system[39,43,51,52]; the triblock co-polymer Pluronic 123 for SBA-15 type matrix with a hexagonal arrangement of cylindrical pores[53,57]; P123 plus *n*-butanol leads to 3D cubic mesoporous KIT-6.[34,57] As an alternative to using surfactants or very large complex organic molecules as templating agents for preparing ordered mesoporous phases, Maschmeyer *et al.*[37,42,45] developed a route with reduced environmental impact and relatively low cost, using simple non-surfactant templating molecules. Specifically, TUD-1 possessing a 3D foam/worm-like mesoporous structure was obtained, with pore widths in the range of 2.5–25 nm, surface areas of up to ca. 1000 m^2 g^{-1}, and relatively good (hydro)thermal stability. Nanocrystalline zeolites have been successfully embedded in the TUD-1 type matrix for different catalytic applications, generally performing better than the corresponding bulk zeolite catalysts: liquid phase alkylation of benzene to ethylbenzene (zeolite Beta),[45] *n*-hexane cracking (Beta),[38] aldol condensation of benzaldehyde with glycol (ZSM-5)[73], acetalization of aldehydes (nano-ITQ-2),[74] and benzylation reactions (H-Y).[55] To the best of our knowledge, there are only two studies of zeolite/TUD-1 composite catalysts for reactions related to biomass valorisation; namely, H-Beta/TUD-1 promoted the acid-catalysed dehydration of D-xylose to furfural (Fur)[44], and conversion of FA (industrially produced via Fur hydrogenation) to LEs.[46]

The valorisation of furfural (Fur) is particularly important for the bio-based economy. Fur is synthesised from the hemicellulose component of lignocellulosic biomass via acid-catalysed hydrolysis and dehydration reactions.[75-77] Industrial production of Fur started in 1921 by the Quaker Oats company,[76] and its importance as a renewable platform chemical for different sectors of the chemical industry is growing. Recent advances in Fur valorisation include integrated reduction and acid reactions of Fur in alcohol medium, via non-H_2 and non-noble metal catalyst approaches, leading to useful bio-based products (furanic ethers (FEs), LA, LEs, angelica lactones (AnLs), γ-valerolactone (GVL)). There are very few catalytic studies on this important reaction system. Román-Bui *et al.*[78] originally used a mechanical mixture of two solid catalysts, namely, Zr-containing (Al-free) Beta type material (for reduction steps) and Brönsted solid acid (for acid reactions); when the solid acid was nanosheets of Al-MFI (surfactant-mediated synthesis) catalytic results were better than when using microcrystalline Al-MFI, which was attributed to enhanced specific surface area and reduced diffusional path lengths in the former case.[78] Recently, we reported nanocrystalline zeotype and TUD-1 type silicates as multifunctional catalysts with favourable textural/morphological characteristics for the integrated conversion of Fur.[79] That study, and others which compared zeolites with amorphous silicate type materials as catalysts for biomass related conversion processes, suggested that metal sites in crystalline frameworks (zeotypes) tend to possess higher intrinsic activity than sites of the same metal located in amorphous frameworks (e.g. TUD-1 type silicates).[78,79,80] Hence, the introduction of adequate active sites into crystalline zeolitic frameworks, and the enhancement of active site accessibility through morphological/textural modifications, may be advantageous in catalyst development for the integrated conversion of Fur.

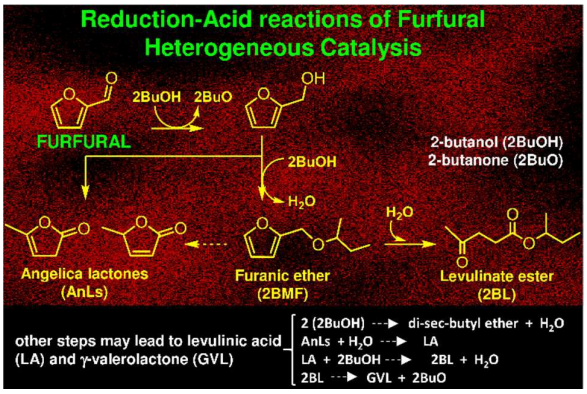

Scheme 1 Catalytic reduction-acid reaction routes involved in the conversion of furfural in alcohol medium, leading to useful bio-products (adapted from refs [79,93]).

In the present work, we explored bulk and composite catalysts which combine Zr,Al-sites, BEA topology and mesoporosity for Fur valorisation via integrated reduction-acid reactions using an alcohol as solvent and H-donor, at 120-150 C (Scheme 1). For the first time, a composite consisting of nanocrystals of Zr,Al-Beta embedded in a mesoporous matrix (ZrAl-Beta /TUD-1) is reported. On the other hand, a bulk mesoporous zeotype, namely MP-ZrAl-Beta-m, prepared via post-synthesis alkaline/acid/SSIE treatments, is investigated for the first time as a bulk catalyst for one-pot reduction/acid reaction systems. The different materials promoted the conversion Fur to useful bio-products (bioP), namely FEs, LEs and AnLs. FEs have applications as blend components of gasoline[81] or aging flavours for beer storage.[82] LEs are interesting as (bio)fuel additives to improve fuel properties and enhance octane or cetane numbers,[83-,85] green solvents,[86] polymers, perfumes, flavours, coatings,[87,88] intermediates for synthesising δ-aminolevulinic acid

View Article Online
DOI: 10.1039/C6CY00223D

(which has shown anticancer, pesticide and insecticide effects).89 ALs can be used as flavouring agents in the food and tobacco industries,[90] as pheromones,[91] and are interesting fuel blending agents.[92]

2. Experimental

2.1 Synthesis of the catalysts

Composite ZrAl-Beta/TUD-1 and nanocrystalline ZrAl-Beta-n. Bulk nanocrystalline (n) ZrAl-Beta-n was prepared from commercially available nanocrystalline NH_4-Beta (Si/Al=12.5, Zeolyst, CP814E) via dealumination (deAl) and solid-state ion-exchange (SSIE), using protocols reported in the literature.[79,93,94] Firstly, NH_4-Beta was converted to the protonic form by calcination at 550 C (heating rate of 1 C min^{-1}) for 10 h in static air, giving H-Beta-n. Afterwards, H-Beta-n was subjected to HNO_3 (70%, Sigma-Aldrich) treatment (20 cm^3 of 13 M aq. HNO_3 per gram of zeolite) at 100 C for 20 h, under stirring; the solid was separated by filtration, thoroughly washed with deionized water until neutral pH, and dried overnight at 65 ºC, giving deAl-Beta-n. With the objective of converting vacant sites formed during the dealumination step, to framework Zr-sites, a solid mixture of deAl-Beta-n and zirconium(IV) acetylacetonate (98%, Sigma-Aldrich, 0.844 mmol Zr per gram of deAl-Beta-n) was gently ground in an agate pestle and mortar, followed by calcination at 550 C (1 C min^{-1}) for 4 h under a flow of air (20 cm^3 min^{-1}), giving ZrAl-Beta-n.

Nanocrystallites of ZrAl-Beta-n were embedded in a mesoporous siliceous TUD-1 type matrix by adapting protocols reported in the literature.[38,42,44,45] According to Hanefeld *et al.*[95] tetraethylammonium hydroxide (TEAOH) is mainly used to refine the structure of TUD-1, but is not essential to the synthesis. Mesoporous TUD-1 type materials have been synthesized using TEAOH/SiO_2 molar ratios in the range of 0.3-1.0.[74,96-105] For ZrAl-Beta/TUD-1, the molar composition of the synthesis mixture of the TUD-1 type matrix was TEOS:TEA:0.9TEAOH:6.6H_2O. Specifically, tetraethylorthosilicate (TEOS, 5.34 g, 25.6 mmol, 98%, Aldrich) was added dropwise to a suspension of ZrAl-Beta-n (1 g) in a mixture of triethanolamine (TEA, 3.85 g, 25.8 mmol, 97%, Fluka) and water (3 g, 0.17 mol), under stirring at room temperature. Then, TEAOH (35 wt.% in water, 9.85 g, 23.4 mmol; Aldrich) was added to the ZrAl-Beta-n-containing mixture, and stirring was continued for 2 h (with gentle heating to 40 ºC, inducing gelation). The gel was aged at room temperature for 24 h, followed by drying at 100 C for 24 h. The obtained solid was gently ground in an agate pestle and mortar, and transferred to a Teflon-lined autoclave and heated at 180 C for 8 h, under static conditions. The autoclave was cooled to room temperature and the solid was subjected to extraction with ethanol (analytical grade, 99.9%, Scharlau, ACS), under reflux for ca. 6 h (using a Soxhlet assembly), similar to a procedure described by Maschmeyer *et al.*[74] The solid was dried overnight at 60 C, gently ground in an agate pestle and mortar, and finally calcined at 600 C (1 C min^{-1}) for 10 h in static air.

Mesoporous silica TUD-1 was prepared in a similar fashion to the composite, but without ZrAl-Beta-n. The ZrO_2 sample used for comparative studies corresponds to that reported in ref.[79]

Mesoporous zeotype MP-ZrAl-Beta-m. The partially dealuminated Zr,Al-containing Beta type material possessing mesoporosity, namely MP-ZrAl-Beta-m (m=microcrystalline; MP=mesoporous), was prepared from a pre-synthesised microcrystalline zeolite H-Beta-m sample, following a similar protocol to that reported recently by Tang *et al.*[106] Mesoporosity can be introduced (at boundaries or defect sites of the zeolite crystals) by silicon removal from the zeolite framework (desilication) via hydrolysis in the presence of OH^-.[15-17,107] Zeolite H-Beta-m was subjected to the following series of post-synthesis treatments: (i) oxalic acid (OxAc) treatment (introducing defect sites); (ii) alkaline treatment to introduce mesoporosity (MP); (iii) strong acid treatment for partial dealumination (deAl) and possible ion-exchange of sodium cations for protons; and (iv) impregnation (or SSIE) of a Zr-precursor and calcination in order to convert vacant sites formed during (iii) to framework Zr-sites, giving MP-ZrAl-Beta-m.

Microcrystalline H-Beta-m was synthesised using TEOS (99.9%, Sigma) as silicon source, and aluminium(III) isopropoxide (≥ 99%, Fluka) as Al-precursor, similar to procedures reported in the literature.[108-110] The molar composition of the synthesis mixture was SiO_2:0.05Al:0.6TEAOH:0.6HF:10H_2O. Specifically, TEAOH (35 wt.% in water, 10.85 g, 25.8 mmol, Aldrich) was added to TEOS (17.69 g, 84.8 mmol) under stirring for 5 h, at room temperature. Afterwards, a solution containing aluminium(III) isopropoxide (0.11 g, 0.53 mmol) and TEAOH (35 wt.% in water, 10.17 g, 24.2 mmol) was added dropwise under vigorous stirring, and the mixture was stirred for a further 20 h. Ethanol formed in the hydrolysis reaction of TEOS was removed at room temperature, under vacuum, for 5 h. Then a solution of HF (50 wt.% in water, 1.74 g, 86.9 mmol, Aldrich) was added to give a gel, which was transferred to a Teflon-lined autoclave and heated at 140 C for 10 days, under static conditions. The obtained solid was washed thoroughly with deionised water, and finally calcined at 580 C (1 C min^{-1}) for 3 h in static air.

The pre-formed H-Beta-m was subjected to the post-synthesis treatments mentioned above. Firstly, a mixture consisting of 20 cm^3 of 0.03 M aq. OxAc (≥99.9%, Aldrich) per gram of H-Beta-m was heated at 70 C for 3 h in a glass vessel equipped with a magnetic stirring bar and a condenser. Then the solid was separated by filtration, thoroughly washed with water until neutral pH, dried at 100 C overnight, and finally calcined at 550 C (1 C min^{-1}) for 5 h in static air, giving OxAc-Beta-m. The solid OxAc-Beta-m was subjected to alkaline treatment by using NaOH (99.3%, JMGS pellets); 20 cm^3 of 0.2 M aq. NaOH per g of zeolite was heated at 65 C for 30 min, in a glass vessel equipped with a magnetic stirring bar and a condenser. The solid was separated by filtration, thoroughly washed with water until neutral pH, and dried at 100 C overnight to give MP-Beta-m. The MP-Beta-m was subjected to acid treatment by using 13 M aq. HNO_3 (70%, Sigma-Aldrich) at 100 C for 20 h. The solid was separated by filtration, thoroughly washed with deionised water until neutral pH, and dried at 60 C overnight, giving deAl-MP-Beta-m. Finally, 0.17 mmol of Zr precursor (zirconium(IV) acetylacetonate) per gram of deAl-MP-Beta-m was gently ground using an agate pestle and mortar, followed by calcination at 550 C (1 C min^{-1}) for 6 h under a flow of air (20 cm^3 min^{-1}), giving MP-ZrAl-Beta-m.

View Article Online
DOI: 10.1039/C6CY00223D

2.2 Characterisation of the catalysts

Powder X-ray diffraction (PXRD) data were collected on an Empyrean PAN analytical diffractometer (Cu-Kα X-radiation, λ = 1.54060 Å) in a Bragg–Brentano para-focusing optics configuration (45 kV, 40 mA). Samples were prepared in a spinning flat plate sample holder and step-scanned in the range from 3.5 to 70° (2θ) with steps of 0.026°. A PIXEL linear detector with an active area of 1.7462 was used with a counting time of 70 s per step. For the TUD-1 type materials, low angle (0.5 - 5° 2θ) PXRD data were collected using the transmission mode, and with the sample deposited between Mylar foils; the samples were step-scanned in 0.013° 2θ steps with a counting time of 80 s per linear detector active area of 2.0 . Scanning electron microscopy (SEM) images, energy dispersive X-ray spectroscopy (EDS) analysis and elemental mappings (Zr, Al, Si) were obtained on a Hitachi SU-70-SEM microscope with a Bruker Quantax 400 detector operating at 20 KV. Transmission electron microscopy (TEM) was carried out on a JEOL 2200FS instrument. Samples were prepared by depositing a drop of a suspension of the solid sample in ethanol onto holey amorphous carbon film-coated 400 mesh copper grids (Agar Scientific). Inductively coupled plasma atomic emission spectroscopy (ICP-AES) analyses were performed at the Central Analysis Laboratory (University of Aveiro); the measurements were carried out on a Horiba JobinYvon Activa W spectrometer (detection limit of ca. 20 μg dm^{-3}; experimental range of error of ca. 5%). Prior to analyses, the solids (10 mg) were digested using 1 cm^3 HF and 1 cm^3 HNO_3, and microwave heating at 180 °C. Nitrogen adsorption-desorption isotherms were measured at -196 C using a Micromeritics ASAP 2010; the samples were pre-treated at 250 C for 3 h. The calculated textural parameters were: specific surface area (S_{BET}) using the BET equation; total pore volume at relative pressure (p/p_0) of ca. 0.98 using the Gurvitsch rule; mesoporous and/or external surface area ($S_{meso/ext}$) and microporous volume (V_{micro}) using the t-plot method. The mesopore size distribution (MSD) curves were calculated from the desorption data using the BJH method.

The thermogravimetric analyses (TGA) and differential scanning calorimetry (DSC) analyses were carried out in air with a heating rate of 10 C min^{-1}, using Shimadzu TGA-50 and DSC-50 instruments, respectively. Prior to analysis, the used solids (after at least 95% Fur conversion was reached) were washed/dried. The amount of carbonaceous matter (wt.% CM) in the used catalysts was based on the mass loss in the temperature range of 250-700 C (no mass loss occurred above ca. 650 C).

The ^{27}Al MAS NMR spectra were recorded at 182.432 MHz using a Bruker Avance III HD 700 (16.4 T) spectrometer with a unique pulse, a recycle delay of 1 s, and a spinning rate of 14 kHz. Chemical shifts are quoted in ppm from $Al(NO_3)_3$.

Fourier transform infrared (FT-IR) spectra were recorded in transmission mode as KBr pellets using a Unican Mattson Mod 7000 spectrometer equipped with a DTGS CsI detector (400-4000 cm^{-1}, 256 scans, 4 cm^{-1} resolution). Diffuse reflectance UV-vis spectra were recorded at room temperature using a dual beam Perkin Elmer 950 spectrometer with a 150 mm diameter Spectralon integrating sphere.

The FT-IR spectra of adsorbed deuterated acetonitrile (CD_3CN) were collected using a NexusThermo Nicolet apparatus (64 scans and resolution of 4 cm^{-1}) equipped with a specially designed cell, using self-supported discs (5-10 mg cm^{-2}). After in situ outgassing at 450 C for 3 h (10^{-6} mbar), the sample was contacted with increasing pressure (2-10 Torr) of CD_3CN (99.80% D), at 30 C, until spectral detection of physisorbed CD_3CN.

The acid properties of the prepared catalysts were measured by FT-IR spectra of adsorbed pyridine, using the same apparatus and sample outgassing procedure as that for FT-IR spectra of adsorbed CD_3CN. After in situ outgassing at 450 C for 3 h (10^{-6} mbar), pyridine (99.99%) was contacted with the sample at 150 C for 10 min, and subsequently evacuated at 150 C and 350 C (30 min), under vacuum (10^{-6} mbar). The IR bands at ca. 1540 and 1455 cm^{-1} are related to pyridine adsorbed on Brönsted (B) and Lewis (L) acid sites, respectively.[111] The evaluation of the acid strength was based on the molar ratios B_{350}/B_{150} (for B acidity), and L_{350}/L_{150} (for L acidity), where L_T and B_T (T= 150 or 350 C) is the amount of L and B acid sites, respectively, remaining in the materials after evacuation at temperature T. The sensitivity limit of the analysis is ca. 5 μmol g^{-1}.

2.3 Catalytic tests

The catalytic experiments were performed in tubular borosilicate batch reactors with pear-shaped bottoms, and equipped with an appropriate PTFE-coated magnetic stirring bar (1000 rpm) and a valve. Each reactor containing 0.45 M furfural (Fur, 99%, Aldrich), 0.75 cm^3 of 2-butanol (99%, Sigma-Aldrich) or 2-propanol (≥99.5%, Sigma-Aldrich), and powdered catalyst (12.9 or 25.7 g_{cat} dm^{-3}) was heated at 120 C or 150 C with a thermostatically controlled oil bath. In some cases, levulinic acid (LA; 98%, Aldrich) and 1-butyl levulinate (1BL; 98%, Aldrich) were used as substrates. Zero time (the instant the reaction began) was taken to be the instant the reactor was immersed in the oil bath. Between batch runs, the reaction mixtures were cooled to room temperature, and the used catalysts were separated by centrifugation, thoroughly washed with 2-butanol and dried at 85 C overnight. The used catalysts were brownish in colour, suggesting the presence of carbonaceous matter (CM). The CM was removed from the solids by calcination at 550 C (1 C min^{-1}) for 3 h, which led to white coloured solids.

The evolution of the catalytic reactions was monitored by GC for quantification of the products formed, and by HPLC for quantification of Fur. The reactors were cooled to ambient temperature before opening and work-up procedures. The analyses were always carried out for freshly prepared samples. The GC analyses were carried out using a Varian 3800 equipped with a capillary column (Chrompack, CP-SIL 5 CB, 50 m x 0.32 mm x 0.5 mm) and a flame ionization detector, using H_2 as carrier gas. The HPLC analyses were carried out using a Knauer Smartline HPLC Pump 100 and a Shodex SH1011 H^+ 300 mm x 8 mm (i.d.) ion exchange column (Showa Denko America, Inc. New York), coupled to a Knauer Smartline UV detector 2520 (254 nm). The mobile phase was 0.005 M aq. H_2SO_4 at a flow rate of 0.8 cm^3 min^{-1}, and the column temperature was 50 C. Calibration curves were measured for quantification. Individual experiments were

View Article Online
DOI: 10.1039/C6CY00223D

performed for a given reaction time and the presented results are the mean values of at least two replicates (error <4%).

The reaction products were identified by GC-MS using a trace GC 2000 Series (Thermo Quest CE Instruments)-DSQ II (Thermo Scientific), equipped with a capillary column (DB-1 MS, 30 m x 0.25 mm x 0.25 μm), using He as carrier gas. The quantified reaction products are furfuryl alcohol (FA), furanic ethers (FEs; 2-butyl furfuryl ether (2BFE) or 2-propyl furfuryl ether (2PFE)), levulinate esters (LEs; 2BL=2-butyl levulinate or 2PL= 2-propyl levulinate), angelica lactones (AnLs=α-angelic lactone plus β-angelic lactone), levulinic acid (LA), and γ-valerolactone (GVL). In general, FEs, LEs and AnLs were mainly formed (bioP refers to FEs, LEs and AnLs). The conversion (%) of substrate (Sub) at a reaction time *t* was calculated using the formula: 100 x [(initial concentration of Sub)-(concentration of Sub at time *t*)]/(initial concentration of Sub). The yield (%) of product (Pro) at a reaction time *t* was calculated using the formula: 100 x [(concentration of Pro at time t)/(initial concentration of Sub)].

3. Results and discussion

3.1 Characterisation of the catalysts

Composite ZrAl-Beta/TUD-1 and nanocrystalline ZrAl-Beta-n. Dealumination of H-Beta-n (Si/Al=12) by HNO_3 treatment gave deAl-Beta-n possessing a Si/Al molar ratio of 591 (ICP-AES, Table 1). The introduction of Zr in deAl-Beta-n gave ZrAl-Beta-n possessing Si/Zr=15. The amount of zeotype component in ZrAl-Beta/TUD-1 is ca. 42 wt.% (based on ICP-AES), which is similar to the theoretical value of ca. 40 wt.% (based on the composition of the synthesis mixture). Hence, ZrAl-Beta-n seems to be completely incorporated in the final composite material. The Zr/Al molar ratio is similar for ZrAl-Beta/TUD-1 (30) and ZrAl-Beta-n (32), suggesting that the procedure to form the composite did not result in leaching of Al or Zr from ZrAl-Beta-n. For each material, the ICP-AES results are roughly comparable to those of EDS, suggesting fairly homogeneous metal dispersions.

Figure 1-a compares the PXRD patterns of ZrAl-Beta/TUD-1 with ZrAl-Beta-n and its synthetic precursors H-Beta-n and deAl-Beta-n. In general, the materials exhibit reflections characteristic of a BEA topology (main peaks at ca. 7.5–8 and 22.4 2θ).[38,112] For all Zr,Al-containing materials prepared, no crystalline phases of zirconia were detected; bulk ZrO_2 exhibited characteristic reflections of the monoclinic phase (ICDD PDF4 + 2013 reference code no. 04-001-7279), with the most intense reflections appearing at 2θ = 28.13 and 31.57 (not observed for the silicates).[113,114] These results suggest fairly homogeneous Zr-dispersion. The low-angle X-ray diffractogram of ZrAl-Beta/TUD-1 is similar to that of TUD-1, showing a broad peak centered at ca. 1.1 2θ (Figure S1 of ESI).[96,115,116] The PXRD results for the composite are consistent with the coexistence of Beta and TUD-1 type phases.

Figure 2 compares the SEM images and elemental (Si, Al, Zr) mappings for ZrAl-Beta/TUD-1 composite, its individual components ZrAl-Beta-n and TUD-1, and mechanically mixed ZrAl-Beta-n+TUD-1. The SEM images and elemental mappings of the synthetic precursors H-Beta-n and deAl-Beta-n are given in Figure S2 (ESI). The synthesis procedures which led to ZrAl-Beta-n did not result in a final morphology considerably different from that of the parent zeolite H-Beta-n. These results are in agreement with literature data for nanocrystalline M-Beta type materials (M=Sn,Al or Zr,Al) prepared in similar fashions.[79,93] The Si, Al and Zr-mappings of ZrAl-Beta-n suggest homogeneous metal dispersions. The images of ZrAl-Beta/TUD-1 are consistent with the dominant morphology being TUD-1 type particles with ZrAl-Beta-n crystals embedded in the silica matrix (Figure 2c). Figure S3 (ESI) exemplifies the morphological differences between the composite and its individual components, i.e. bulk ZrAl-Beta-n (composed of aggregates of pseudospherical particles, in agreement with literature data[79]) and amorphous silica TUD-1 (composed of particles with irregular shapes and sizes, in agreement with literature data[79,95,113]). For mechanically mixed ZrAl-Beta-n+TUD-1, separate particles were observed that correspond to pure ZrAl-Beta-n (e.g., particle A in Figure 2d and e) and TUD-1 (e.g., particle B in Figure 2d and e). The Zr-mapping of the composite (Figure 2c) qualitatively points towards a lower Zr concentration than for bulk ZrAl-Beta-n (Figure 2a), which is consistent with the higher Si/Zr ratio of the former (Table 1).

Table 1 Compositions of the prepared materials

Sample[a]	Molar compositions (ICP-AES)				Molar compositions (EDS)			
	Si/Al	Si/Zr	Zr/Al	Si/(Zr+Al)	Si/Al	Si/Zr	Zr/Al	Si/(Zr+Al)
Nanocrystalline/Composite materials								
H-Beta-n	12	-	-	-	10	-	-	-
deAl-Beta-n	463	-	-	-	406	-	-	-
ZrAl-Beta-n	474	15	32	15	459	19	24	18
ZrAl-Beta/TUD-1	1589	53	30	51	1607	50	32	49
ZrAl-Beta/TUD-1 used[b]	1373	45	31	44	1337	40	33	39
Microcrystalline/Mesoporous materials								
H-Beta-m	20	-	-	-	19	-	-	-
OxAc-Beta-m	50	-	-	-	46	-	-	-
MP-Beta-m	33	-	-	-	32	-	-	-
deAl-MP-Beta-m	285	-	-	-	257	-	-	-
MP-ZrAl-Beta-m	320	86	4	68	284	88	4	67
MP-ZrAl-Beta-m-used[b]	309	89	4	69	271	90	3	67

[a] In the sample names, n stands for nanocrystalline, m for microcrystalline, deAl for partially dealuminated, and MP for mesoporous. [b] Catalyst recovered from catalytic reaction of Fur/2BuOH, at 150 C.

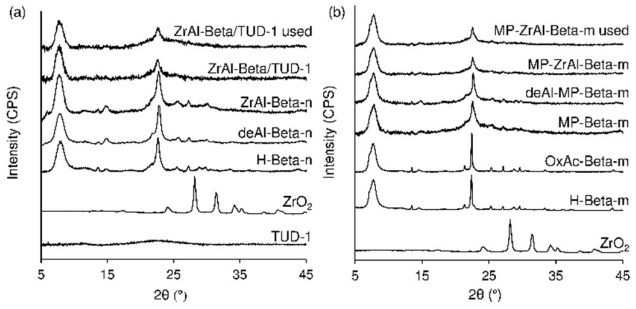

Figure 1 PXRD patterns for: (a) composite ZrAl-Beta/TUD-1 (fresh and recovered after Fur conversion), nanocrystalline ZrAl-Beta-n and its synthetic precursors, and TUD-1; (b) MP-ZrAl-Beta-m and its synthetic precursors. Results for bulk zirconia (ZrO_2) are included for comparison.

View Article Online
DOI: 10.1039/C6CY00223D

The high-resolution (HR) TEM images of H-Beta-n show ca. 20-30 nm sized crystallites (and characteristic lattice fringes) which are clustered into larger particles (Figure 3b). These features are common to ZrAl-Beta-n (Figure 3c and 3d) suggesting that the crystalline structure was essentially preserved during the modification treatments. The TEM images of ZrAl-Beta/TUD-1 are consistent with a composite of ZrAl-Beta-n nanocrystals embedded within a mesoporous silica (amorphous) matrix of the type TUD-1 (Figures 3e and 3f). Regions containing clusters or aggregates of nanocrystals up to 200 nm in size within the TUD-1 type matrix were observed. Similar morphological features were reported previously for composites of the type H-Beta/TUD-1 possessing a similar zeolite loading (ca. 40 wt.%) to that for ZrAl-Beta/TUD-1).[38,44]

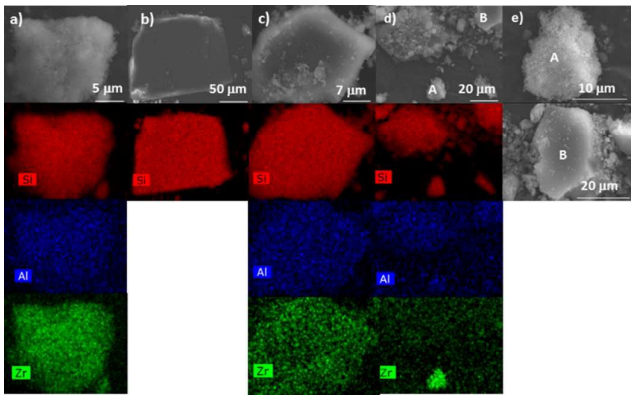

Figure 2 SEM and elemental (Si, Al, Zr) mapping for (a) ZrAl-Beta-n, (b) TUD-1, (c) ZrAl-Beta/TUD-1, (d) mechanically mixed ZrAl-Beta-n+TUD-1, and (e) enlargement of the SEM images of particles A and B.

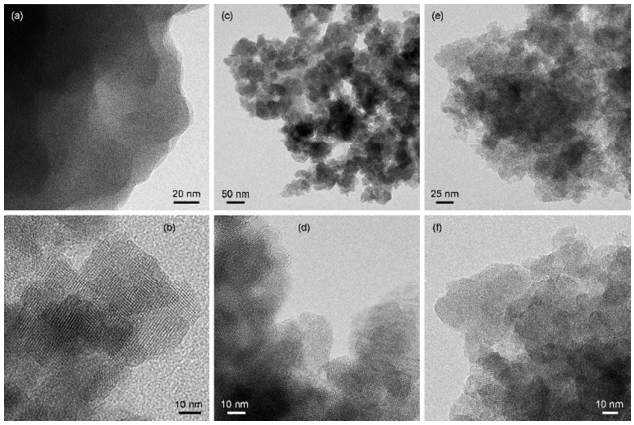

Figure 3 TEM images of (a) TUD-1, (b) H-Beta-n, (c and d) ZrAl-Beta-n, and (e and f) ZrAl-Beta/TUD-1. The amorphous carbon support film used for H-Beta-n appears as the mottled background in the upper and lower right-hand parts of the micrograph; a holey carbon film was used for the other samples.

Figure 4-a compares the N_2 adsorption-desorption isotherms of the materials, and the corresponding textural parameters are given in Table 2. Zeolite H-Beta-n and its modified versions deAl-Beta-n and ZrAl-Beta-n, exhibited type I isotherms, characteristic of microporous materials (Figure 4-a). Significant N_2 uptake at high relative pressures (p/p_0) was observed and is likely to be due to multilayer adsorption on the external surface. The S_{BET} of H-Beta-n decreased after the modification treatments, particularly dealumination (from 705 $m^2\ g^{-1}$ for H-Beta-n to 525-587 $m^2\ g^{-1}$ for deAl-Beta-n and ZrAl-Beta-n). The three materials possessed considerable external surface area (179-245 $m^2\ g^{-1}$), in agreement with literature data for similarly prepared nanocrystalline materials.[79,93,94] For ZrAl-Beta/TUD-1 and TUD-1, the isotherms present features of the type IV, and a hysteresis loop, characteristic of mesoporous materials. Similar isotherms were reported in the literature for TUD-1 type materials,[117,118] and composites of H-ZSM-5[73], Beta[38] or ITQ-2[74] embedded in TUD-1 type matrix. Composite ZrAl-Beta/TUD-1 possessed enhanced S_{BET}, S_{meso} and V_p in relation to bulk ZrAl-Beta-n, which can be mainly attributed to the mesoporous component of the composite. On the other hand, V_{micro} of ZrAl-Beta/TUD-1 is significantly higher than that of TUD-1 (0.14 and 0.06 cm^3/g, respectively), and equal to that of ZrAl-Beta-n, suggesting that the microporosity in the composite is mainly associated with the zeotype component. The mesopore size distribution curves of ZrAl-Beta/TUD-1 and TUD were broad, with median at ca. 26 nm (inset of Figure 4-a). Comparable results have been described in a patent for these types of materials.[42]

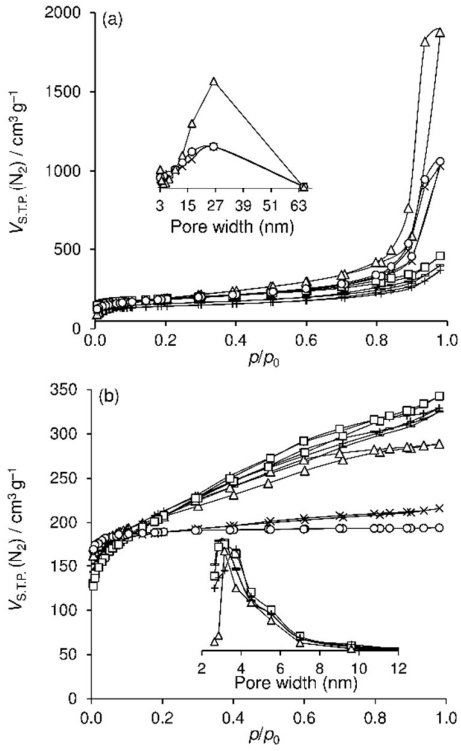

Figure 4 N_2 adsorption-desorption isotherms at -196 C for: (a) (□) H-Beta-n, (-) deAl-Beta-n, (+) ZrAl-Beta-n, (x) ZrAl-Beta/TUD-1, (o) ZrAl-Beta/TUD-1 used, (Δ) TUD-1 (the mesopore size distribution curves for ZrAl-Beta/TUD-1 (fresh and recovered after Fur conversion) and TUD-1 are given in the inset, with matching symbols); (b) (o) H-Beta-m, (×) OxAc-Beta-m, (Δ) MP-Beta-m, (+) deAl-MP-Beta-m, (-) MP-ZrAl-Beta-m and (□) MP-ZrAl-Beta-m used (the mesopore size distribution curves for MP-Beta-m, deAl-MP-Beta-m, MP-ZrAl-Beta-m (fresh and recovered after Fur conversion) are given in the inset, with matching symbols). The lines are visual guides.

View Article Online
DOI: 10.1039/C6CY00223D

Table 2 Textural properties of the prepared materials.

Sample[a]	S_{BET} ($m^2 g^{-1}$)	$S_{meso/ext}$ ($m^2 g^{-1}$)	V_{micro} ($cm^3 g^{-1}$)	V_p ($cm^3 g^{-1}$)
Nanocrystalline/Composite materials				
H-Beta-n	705	245	0.19	0.71
deAl-Beta-n	587	205	0.15	0.62
ZrAl-Beta-n	525	179	0.14	0.58
TUD-1	683	575	0.06	2.9
ZrAl-Beta/TUD-1	704	321	0.15	1.59
ZrAl-Beta/TUD-1 used[b]	679	335	0.14	1.64
Microcrystalline/Mesoporous materials				
H-Beta-m	764	9	0.29	0.30
OxAc-Beta-m	744	53	0.27	0.33
MP-Beta-m	760	296	0.19	0.45
deAl-MP-Beta-m	767	319	0.19	0.51
MP-ZrAl-Beta-m	746	310	0.19	0.50
MP-ZrAl-Beta-m used[b]	741	361	0.17	0.53

[a] In the sample names, n stands for nanocrystalline, m for microcrystalline, deAl for partially dealuminated, and MP for mesoporous. [b] Catalyst recovered from catalytic reaction of Fur/2BuOH, at 150 C.

The materials ZrAl-Beta/TUD-1 and ZrAl-Beta-n exhibited very different FT-IR (Figure 5-a) and DR UV-vis (Figure S4-a) spectral features from bulk ZrO_2, suggesting that the SSIE for Zr to give ZrAl-Beta-n, and, on the other hand, the embedment of ZrAl-Beta-n in the mesoporous matrix did not lead to formation of zirconium oxide particles (consistent with PXRD). Figure 5-a compares the FT-IR spectra of ZrAl-Beta/TUD-1, ZrAl-Beta-n and its synthetic precursors. In general, the materials exhibit the main spectral features of Beta type zeolite, and small differences between the materials are associated with the modification treatments. H-Beta-n exhibits main bands at 1228 cm^{-1} attributed to internal asymmetric stretching vibrations of [TO_4] tetrahedra (T=Si, Al), 1093 cm^{-1} and 796 cm^{-1} attributed to external asymmetric and symmetric stretching vibrations, respectively, of [TO_4] tetrahedra; 620 cm^{-1}, 574 cm^{-1} and 522 cm^{-1} attributed to double ring external vibrations of [TO_4] tetrahedra, and 464 cm^{-1} attributed to internal T-O bending vibrations of [TO_4] tetrahedra).[108,113,114,119-122] The band at 426 cm^{-1} is assigned to pore opening vibrations.[114,122] For deAl-Beta-n, changes in relative intensities of the bands at 575 cm^{-1} and 525 cm^{-1} (characteristic of zeolite Beta) were observed, possibly associated with the removal of framework Al species.[108,113,123] A band at 951 cm^{-1} is assigned to Si–O stretching vibrations of Si–OH groups present at connectivity defects formed during the dealumination process.[79,108,113] For ZrAl-Beta-n, the relative intensity of the band at 951 cm^{-1} was lower than for deAl-Beta-n, suggesting a lower amount of connectivity defects in the former material, and the insertion of Zr at defect sites of deAl-Beta-n.[79,93,108] The spectrum of ZrAl-Beta/TUD-1 is similar to that of ZrAl-Beta-n, suggesting that the chemical structure of ZrAl-Beta-n was essentially preserved under the conditions used to synthesise the composite. ZrAl-Beta/TUD-1 and ZrAl-Beta-n exhibited different spectral features from bulk ZrO_2, suggesting the absence of zirconium oxide particles in the prepared materials (consistent with PXRD and DR UV-vis).

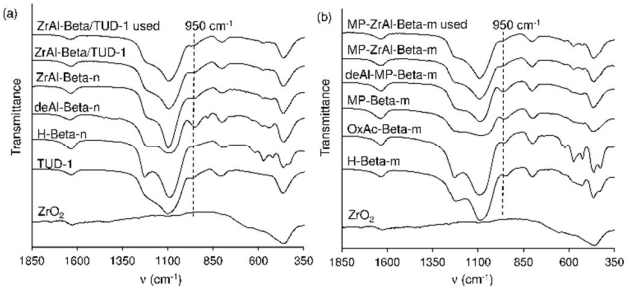

Figure 5 FT-IR spectra of (a) composite ZrAl-Beta/TUD-1 (fresh and recovered after Fur conversion), ZrAl-Beta-n and its synthetic precursors, bulk ZrO_2 and TUD-1; (b) MP-ZrAl-Beta-m (fresh and recovered after Fur conversion), its synthetic precursors, and ZrO_2.

The materials were characterised by FT-IR of adsorbed deuterated acetonitrile (CD_3CN) to help gain insights into the chemical nature of the Zr-sites (Figure 6). According to the literature, CD_3CN may interact with framework Zr-sites, and not with zirconium oxide particles.[124] It was reported in the literature for Zr-containing beta type zeolites that the tetrahedral Zr-species may be closed-sites (Zr-$(OSi)_4$) or open-sites (Zr-$(OSi)_3(OH)$, where the hydroxyl ligand may be formed via Zr-O-Si scissoring.[124,134-137] ZrAl-Beta/TUD-1 and ZrAl-Beta-n exhibited bands at ca. 2303 and 2274 cm^{-1} (Figure 6-a). The band at ca. 2303 cm^{-1} is assigned to C≡N bond stretching vibrations of CD_3CN coordinated with framework zirconium closed-sites.[124] The band centred at ca. 2274 cm^{-1} is due to CD_3CN interacting with Si-OH groups.[125,126] The relative intensity of the band at 2274 cm^{-1} was higher for the composite than ZrAl-Beta-n, possibly due to enhanced contribution of the siliceous matrix with silanol groups. Increasing the CD_3CN coverage did not lead to significant shifts in the band maxima, and a weak shoulder appears at ca. 2268 cm^{-1} due to physisorbed CD_3CN (exemplified for ZrAl-Beta-n in Figure 6-b).

According to the literature, Sn-containing Beta zeotype prepared via hydrothermal synthesis[125], or via post-synthesis treatments (dealumination and introduction of Sn-species)[127], exhibit bands at ca. 2308 and ca. 2316 cm^{-1} due to CD_3CN adsorbed on tin closed- and open-sites, respectively. ZrAl-Beta/TUD-1 and ZrAl-Beta-n did not exhibit a spectral band at ca. 2316 cm^{-1}. However, we cannot fully exclude the possibility of existing zirconium open-sites in the materials prepared, in agreement with detailed vibrational spectroscopic studies reported by Irina and coworkers, for (Al-free) Zr-Beta (synthesised via fluoride-based hydrothermal method).[124]

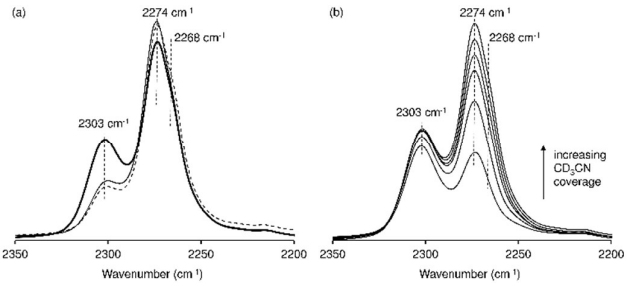

Figure 6 FT-IR spectra of CD_3CN adsorbed on (a) ZrAl-Beta-n (thick line), ZrAl-Beta/TUD-1 (thin line) and MP-ZrAl-Beta-m (dashed line), or (b) ZrAl-Beta-n with increasing coverage.

View Article Online
DOI: 10.1039/C6CY00223D

The nature of the Al species in the prepared materials was investigated by ^{27}Al MAS NMR spectroscopy (Figure 7-a). Zeolite H-Beta-n exhibited a predominant resonance at ca. 54 ppm due to aluminium species in tetrahedral coordination (Al_{tetra}), and a weak resonance at ca. 0 ppm due to aluminium species in octahedral coordination (Al_{octa}) which may be extra-framework species or species connected to the framework and formed from Al_{tetra}.[108,128-133]. The spectrum of deAl-Beta-n displays an Al_{tetra} signal, but no peak at 0 ppm could be distinguished. The spectrum of ZrAl-Beta-n is similar to that of deAl-Beta-n, suggesting that SSIE/calcination did not affect Al_{tetra} (Figure 7-a). The composite ZrAl-Beta/TUD-1 exhibited a broad signal in the region associated with Al_{tetra}; the spectrum is poorly resolved due to the very low Al concentration (Table 1). In general, the signal assigned to Al_{tetra} is somewhat broad, indicating chemical distributions of framework $Al(OSi)_4$ groups with varying bond angles and lengths, possibly at different crystallographic positions of the zeolite framework.[128,130,131] In summary, ZrAl-Beta/TUD-1 and ZrAl-Beta-n seem to possess essentially Al_{tetra} (responsible for Brönsted acidity).

Table 3 compares the acid properties of ZrAl-Beta/TUD-1 and ZrAl-Beta-n measured by FT-IR of adsorbed pyridine, at 150 C. The two materials possessed Brönsted acid sites (B), and mostly Lewis acid sites (L). The composite possessed lower total amount of acid sites (L+B) than the bulk zeotype, likely due to dilution effects; ZrAl-Beta/TUD-1 consists of a zeotype component dispersed in a siliceous matrix. For the two materials, evacuation at 350 C led to considerable decrease in the amount of adsorbed pyridine (L_{350}/L_{150}=0.1 and B_{350}/B_{150}=0), suggesting that most of the L and B acid sites are relatively weak. ZrAl-Beta/TUD-1 and ZrAl-Beta-n possess similar acid strengths (L_{350}/L_{150} as well as B_{350}/B_{150} were the same for the two materials).

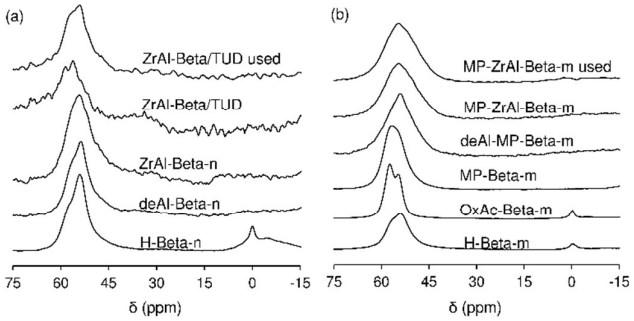

Figure 7 ^{27}Al MAS NMR spectra of: (a) the composite ZrAl-Beta/TUD-1 (fresh and recovered after Fur conversion), ZrAl-Beta-n and its synthetic precursors; (b) MP-ZrAl-Beta-m and its synthetic precursors.

Table 3 Acid properties of the Zr,Al-containing materials.[a]

Sample	L (μmol g^{-1})	B (μmol g^{-1})	L+B (μmol g^{-1})	L/B
ZrAl-Beta-n	106	36	142	2.9
ZrAl-Beta/TUD-1	79	16	95	4.8
MP-ZrAl-Beta-m	73	10	83	7.5

a Determined by FT-IR of adsorbed pyridine, at 150 C; B=Brönsted acid sites, L=Lewis acid sites, B+L=total amount of acid sites.

The measured amounts of B and L acid sites of the composite were compared to the corresponding values (theoretical) calculated for 42 wt% loading of ZrAl-Beta-n (using the measured values for ZrAl-Beta-n, Table 3). The measured amount of B acid sites of ZrAl-Beta/TUD-1 (16 μmol g^{-1}, Table 3) is similar to the calculated value (15 μmol g^{-1}). These results suggest that the B acidity of ZrAl-Beta-n was not significantly affected by the in situ synthesis of the mesoporous matrix. The composite seems to possess enhanced L acidity, since the measured amount (79 μmol g^{-1}) was higher than the calculated value (45 μmol g^{-1}). Pristine silica TUD-1 and bulk zirconia were analysed for comparative studies, and possessed negligible acidity. Hence, the enhanced L acidity of ZrAl-Beta/TUD-1 is associated with framework species of the zeotype component. It was reported in the literature for Zr-containing beta type zeolites, that framework zirconium closed-sites and open-sites may act as L acid sites (open-sites may be stronger L sites), and the open-sites may also contribute with B acidity.[124,134-136] Accordingly, conversion of closed-sites into open-sites may lead to enhanced amount of B sites without affecting considerably the amount of L acid sites, and the L acid strength may be enhanced. These trends in acid properties were not observed for the composite ZrAl-Beta/TUD-1 in relation to the bulk material ZrAl-Beta-n. Overall, the results suggest that the synthesis conditions of the TUD-1 type matrix did not significantly influence the surface chemistry of the zeotype component. The enhanced amount of L acid sites of the composite may be partly due to favourable nanocrystallites dispersion effects in comparison to bulk (aggregated) ZrAl-Beta-n.

Mesoporous zeotype MP-ZrAl-Beta-m. The synthesised zeolite H-Beta-m possessed a Si/Al molar ratio of 20 (Table 1), which is in the range of values considered favourable for post-synthesis alkaline treatment without drastic loss of crystallinity.[106,123,138,139] For example, Tian *et al.*[122] reported that the crystallinity could be retained when treating Beta zeolites possessing Si/Al molar ratios in the range of 14.5-21 with 0.2 M NaOH (similar to that used in the present work). The oxalic acid treatment (step (i)) led to OxAc-Beta-m possessing higher Si/Al ratio (50), in agreement with literature data for similarly modified zeolite Beta.[106,123,140] The alkaline treatment (step (ii)) gave MP-Beta-m possessing a reduced Si/Al ratio of 33 due to desilication. Subsequent HNO_3 treatment (step (iii)) led to deAl-MP-Beta-m with an enhanced Si/Al ratio of 285 due to dealumination. The SSIE for Zr gave MP-ZrAl-Beta-m with Si/Zr = 86 (Zr/Al = 4), and a comparable Si/Al ratio to deAl-Beta-n.

Figure1-b compares the PXRD patterns of MP-ZrAl-Beta-m and its synthetic precursors. The PXRD patterns of H-Beta-m and OxAc-Beta-m are similar, showing characteristic reflections of BEA topology; predominantly 7.7 and 22.4 2θ, and less intense peaks at 13.5 , 14.5 , 21.3 , 25.3 , 27.1 , 28.7 , 29.5 , 33.3 and 43.5 2θ.[38,108,112,121,141] The stability of zeolite Beta towards the oxalic acid treatment is in agreement with that reported by Tang *et al.*[106] and Tian *et al.*[123] MP-Beta-m exhibited the two main reflections characteristic of zeolite Beta (7.7 and 22.7 2θ), while weaker reflections were hardly distinguished, suggesting partial loss of crystallinity during the alkaline treatment. Similar results were reported previously for similarly treated Beta materials.[123,139,142,143] Subsequent dealumination and SSIE for Zr did not significantly affect the crystalline structure. No crystalline phases of zirconia, alumina and/or silica were found in the PRXD patterns of the

View Article Online
DOI: 10.1039/C6CY00223D

prepared materials, suggesting fairly homogeneous metal dispersions.

Figure 8 shows the SEM images and elemental mappings of MP-ZrAl-Beta-m and its synthetic precursors. Zeolite H-Beta-m consists of ca. 2 μm size crystals, possessing a truncated square bypiramidal structure. Similar morphology has been reported in the literature for microcrystalline zeolite H-Beta.[108,144-146] The morphological characteristics of H-Beta-m are comparable to those of the modified materials, excluding MP-ZrAl-Beta-m which had a less regular morphology. Elemental mappings of H-Beta-m, OxAc-Beta-m and MP-Beta-m suggest homogeneous dispersions of Si and Al. For deAl-MP-Beta-m and MP-ZrAl-Beta-m, the Al and (Zr,Al) dispersions, respectively, seem to be homogeneous; the poor level of colour contrast of these mappings is likely due to the low Al and Zr concentrations.

The N_2 adsorption-desorption isotherms and textural properties of MP-ZrAl-Beta-m and its synthetic precursors are given in Figure 4-b and Table 2, respectively. Precursors H-Beta-m and OxAc-Beta-m exhibited type I isotherms, characteristic of microporous materials. MP-Beta-m exhibited type IV isotherm features, and a hysteresis loop, characteristic of mesoporous materials (Figure 4-b). In comparison to OxAc-Beta-m, MP-Beta-m possessed enhanced S_{meso} (296 $m^2\ g^{-1}$) and reduced V_{micro} (0.19 $cm^3\ g^{-1}$) (Table 2). The S_{meso} for MP-Beta-m is in the range of values reported in the literature for alkaline treated microcrystalline H-Beta (increases from 20-128 m^2/g for the parent zeolites to 336-510 $m^2\ g^{-1}$ for the corresponding treated materials).[12,123,138,139,147,148] From OxAc-Beta-m to MP-Beta-m, the decrease of V_{micro} was equal to the increase of V_p. Hence, for MP-Beta-m, the difference between V_p and V_{micro} likely corresponds to intracrystalline mesoporous volume. Further modification treatments leading to deAl-MP-Beta-m (dealumination) and MP-ZrAl-Beta-m (SSIE for Zr) did not lead to considerable changes in textural properties. The mesopore size distribution curves of MP-Beta-m, deAl-MP-Beta-m and MP-ZrAl-Beta-m were comparable, and centred in the range of ca. 3-4 nm (inset of Figure 4-b). In general, these results parallel those reported by Tang *et al.*[106] for similarly prepared materials.

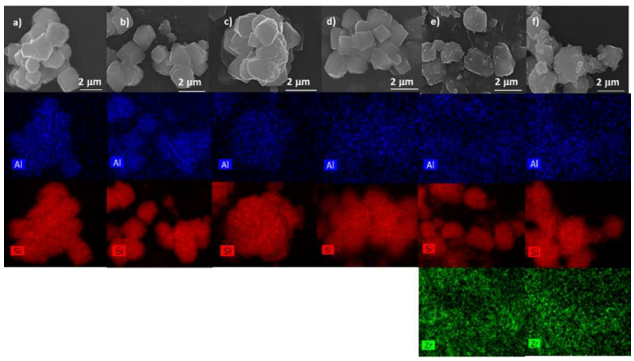

Figure 8 SEM and elemental mapping of a) H-Beta-m, b) OxAc-Beta-m, c) MP-Beta-m, d) deAl-MP-Beta-m, e) MP-ZrAl-Beta-m and f) MP-ZrAl-Beta-m used.

MP-ZrAl-Beta-m exhibited very different FT-IR (Figure 5-b) and DR-UV-vis (Figure S4-b) spectral features from bulk ZrO_2, suggesting that the SSIE for Zr did not lead to the formation of zirconium oxide particles. In general, the materials exhibited the main FT-IR spectral features characteristic of Beta type zeolite (the band assignments match those discussed above for nanocrystalline H-Beta-n and related materials) (Figure 5-b).[108,113,121,149] The modification treatments led to small spectral differences. Enhanced relative intensities of the bands at 575 cm^{-1} and 525 cm^{-1} for OxAc-Beta-m may be associated with partial dealumination.[108,113,123] For MP-Beta-m, the less resolved bands in the range of 460-620 cm^{-1} and the disappearance of the band at 426 cm^{-1} indicate that changes occurred in the framework during the desilication process. The SSIE for Zr (MP-ZrAl-Beta-m) led to a decrease in the relative intensity of the band at 952 cm^{-1} ascribed to silanol defect sites, suggesting the successful introduction of (tetrahedral) Zr in the zeolite framework.[79,108,150] On the other hand, the enhanced relative intensity of the band at 578 cm^{-1} for MP-ZrAl-Beta-m may be due to enhanced framework vibrations after the SSIE process, in agreement with literature data.[94,108]

The type of framework Zr-sites of MP-ZrAl-Beta-m was investigated by FT-IR of adsorbed deuterated acetonitrile (CD_3CN) (Figure 6). MP-ZrAl-Beta-m exhibited bands at ca. 2274 and 2303 cm^{-1} assignable to Si-OH groups and zirconium closed-sites, respectively.[124-126] The IR spectra are similar for MP-ZrAl-Beta-m and the composite.

Figure 7-b compares the ^{27}Al MAS NMR spectra for MP-ZrAl-Beta-m and its synthesis precursors. The spectrum of the parent zeolite H-Beta-m shows a strong resonance centred at ca. 54 ppm due to Al_{tetra}, and a weak resonance at 0 ppm attributed to Al_{octa}. The latter resonance disappears after desilication (MP-Beta-m), and does not reappear after dealumination (deAl-MP-Beta-m) or SSIE for Zr (MP-ZrAl-Beta-m); these materials exhibited a single broad peak associated with Al_{tetra} (responsible for Brönsted acidity). According to the literature, alkaline treatments may lead to reinsertion of extra-framework aluminum into the framework.[151] The signals assigned to Al_{tetra} are broad and may comprise overlapping resonances (e.g. two resolved resonances are observed for OxAc-Beta-m at ca. 54 and 57 ppm), indicating chemical distributions of framework $[Al(OSi)_4]$ groups with varying bond angles and lengths.[128,130,131]

MP-ZrAl-Beta-m possesses B and mostly L acidity, ascertained by FT-IR spectroscopy of pyridine adsorbed on the material (Table 3). Evacuation at 350 C led to considerable decrease in the amount of adsorbed pyridine; L_{350}/L_{150}=0.1 and B_{350}/B_{150}=0, suggesting that the B acid sites and most of the L acid sites are relatively weak. MP-ZrAl-Beta-m is comparable to ZrAl-Beta/TUD-1 and ZrAl-Beta-n in terms of acid strength.

A comparative study for the three Zr-containing materials prepared indicated that the total amount of acid sites (L+B) tended to increase with the molar ratio (Zr+Al)/Si (Tables 1 and 3), consistent with surface acidity being associated with Zr- and Al-sites. On the other hand, the amount of L acid sites (Table 3) increased with the molar ratio Zr/Si (linear relationship, R^2=0.998 (not shown)), suggesting that the L acidity is essentially associated with Zr-sites. This hypothesis is somewhat supported by the very low molar ratios Si/Al (Table 1), and the ^{27}Al MAS NMR studies (the materials exhibited no clearly distinguishable peak at ca. 30 ppm due to L acid aluminium sites, Figure 7). Accordingly, the measured L acidity of the three Zr-containing materials prepared may be essentially associated with framework Zr-sites, which are known to possess

View Article Online
DOI: 10.1039/C6CY00223D

intrinsic catalytic activity for Fur conversion.[78,110] Based on the above considerations, tentative relationships between the catalytic results and Zr-sites were made using turnover frequencies calculated per amount of L acid sites.

3.2 Catalytic studies

Composite ZrAl-Beta/TUD-1. The reaction of Fur in the presence of the composite ZrAl-Beta/TUD-1, using 2-butanol (2BuOH) with the dual function as solvent and H-donor, in the temperature range 120-150 C, gave mainly the bio-products (bioP) 2-butyl furfuryl ether (2BFE), 2-butyl levulinate (2BL) and angelica lactones (AnLs), which were formed with total yields of up to 93% at 96% Fur conversion (Figures 9 and S5). Other reaction products included furfuryl alcohol (FA), levulinic acid (LA) and γ-valerolactone (GVL) which were always formed in less than 2% yield each. The reaction of Fur without catalyst at 150 C was sluggish (20% conversion and negligible bioP yields at 24 h), affirming the catalytic role of ZrAl-Beta/TUD-1 in Fur conversion.

The composite ZrAl-Beta/TUD-1 led to a similar product spectrum to that reported in the literature (to the best of our knowledge, there are only two studies) for Zr-containing Beta type materials tested as catalysts under similar Fur reaction conditions, namely $(Zr)_{SSIE}$-Beta sample of ref.[79] which was prepared in a similar fashion to ZrAl-Beta-n; and mechanically mixed (Al-free) Zr-Beta and (Zr-free) Al-MFI-ns of ref.[78] in which Zr-Beta was synthesised via HF-based prolonged hydrothermal synthesis, and Al-MFI-ns consisted of nanosheets with MFI topology obtained via surfactant-mediated hydrothermal synthesis. The fact that the product spectrum was similar for the three catalytic systems suggests that a similar overall reaction mechanism is involved. The overall reaction of Fur may involve catalytic transfer hydrogenation (CTH) where the alcohol solvent simultaneously acts as H-donor, and acid-catalysed reactions indicated in Scheme 1.[79,93] The CTH steps include Fur-to-FA conversion[152-154] (initialising the cascade reaction process) and, further down the cascade process, 2BL-to-GVL conversion.[78,79,93,137,155] The low FA yields (<2%) observed for ZrAl-Beta/TUD-1 is an indication of its high reactivity, undergoing acid-catalysed reactions.[79,93] The acid-catalysed steps include an etherification reaction between FA and 2-butanol to give 2BFE, ring-opening of 2BFE to give 2BL, an esterification reaction between LA and 2-butanol to give 2BL, isomerisation of FA to AnLs, conversion of 2BFE to AnLs, and hydration of AnLs to give LA (Scheme 1). The effectiveness of ZrAl-Beta/TUD-1 for the Fur-to-bioP conversion is an indication that it possesses adequate active sites for the reduction and acid chemistry involved. The Zr-sites may promote the CTH steps, and, on the other hand, the Zr- and Al-sites may promote the acid-catalysed steps, with Al-sites enhancing the steps FA-to-AnLs, 2BFE-to-AnLs, ring-opening reaction of 2BFE-to-2BL, and esterification of LA-to-2BL.[78,79,93] Accordingly, the high Zr/Al molar ratio (Table 1) of ZrAl-Beta/TUD-1 at least partly explains the fact that the predominant bioP is 2BFE.

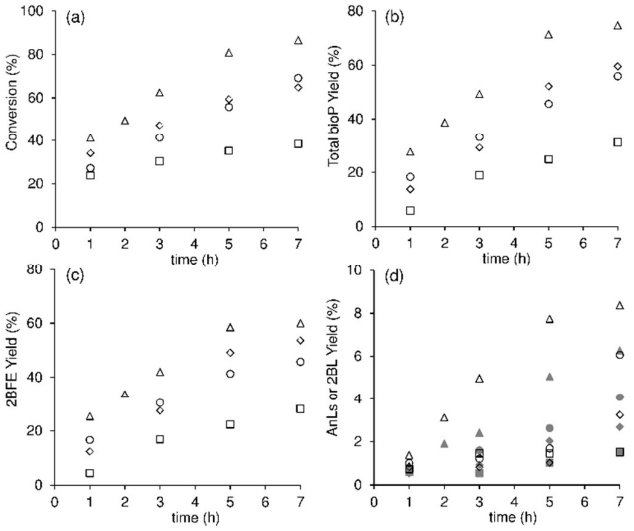

Figure 9. Influence of reaction temperature (T) and catalyst load (CatLoad) on (a) Fur conversion, (b) total bioP yield, (c) 2BFE yield, and (d) AnLs (unfilled symbols) and 2BL (grey symbols) yields, in the presence of ZrAl-Beta/TUD-1, using 2-butanol as solvent and H-donor: (squares) T=120 C, CatLoad=12 9 g_{cat} dm^{-3}; (circles) T=120 C, CatLoad=25.7 g_{cat} dm^{-3}; (diamonds) T=150 C, CatLoad=12.9 g_{cat} dm^{-3}; (triangles) T=150 C, CatLoad=25.7 g_{cat} dm^{-3}.

It has been reported that bulk ZrO_2 was ineffective for the reaction of Fur, and that the active Zr-sites of ZrAl-containing Beta type catalysts are framework species.[78,110] The catalytic performance of ZrAl-Beta/TUD-1 was compared to that of (Zr-free) composite H-Beta/TUD-1; this sample was previously tested and effective for the acid-catalysed conversion of xylose to Fur, at 170 C.[44] The reaction of Fur in the presence of H-Beta/TUD-1 was sluggish (5% total bioP yield at 44% conversion, 24 h; T=150 C, CatLoad=25.7 g_{cat} dm^{-3}) compared to ZrAl-Beta/TUD-1 (75% total yield at 97% conversion, 24 h). These results are consistent with the determinant role of Zr-sites in triggering the cascade reaction process via the CTH step Fur-to-FA (which leads to the bioP). Based on the characterisation studies and in agreement with the literature, tetrahedral (framework) Zr-sites are likely the active Lewis acid sites of the Fur-to-FA conversion.[78,110]

The alcohol solvent acts simultaneously as H-donor in the CTH steps. Besides 2BuOH, 2-propanol (2PrOH) has been identified as an effective H-donor solvent for the conversion of carbohydrate biomass-derived chemicals.[93,155,156] The reaction of Fur with 2PrOH in the presence of ZrAl-Beta/TUD-1 gave furfuryl 2-propyl ether (2PFE), 2-propyl levulinate (2PL) and AnLs, which parallels the product spectrum of the Fur/2BuOH system (T=120 C, CatLoad=25.7 g_{cat} dm^{-3}, Figure S6). The dependence of total bioP yield on conversion was roughly coincident for the two alcohols (Figure S6-b), although the reaction of Fur was slower in 2PrOH than in 2BuOH (42% and 69% conversion at 7 h, respectively, Figure S7-a). These results somewhat parallel literature data reported by our group for a Sn,Al-containing Beta type catalyst tested under identical Fur reaction conditions[93], suggesting that 2BuOH is a favourable H-donor solvent for this reaction system.

The influence of the catalyst load (CatLoad) and temperature (T) on the Fur/2BuOH reaction in the presence of ZrAl-Beta/TUD-1 is shown in Figure 9. For T=120 C and CatLoad=12.9 g_{cat} dm^{-3} the

View Article Online
DOI: 10.1039/C6CY00223D

reaction was relatively slow (39% conversion and 31% total bioP yield, at 7 h). Increasing the CatLoad from 12.9 to 25.7 g_{cat} dm^{-3} at 120 C was kinetically favourable (69% conversion and 56% total bioP yield, at 7 h). A similar trend in kinetics was observed when increasing T from 120 to 150 C, using a CatLoad of 12.9 or 25.7 g_{cat} dm^{-3}. The set of reaction conditions (T=150 C, CatLoad=12.9 g_{cat} dm^{-3}) and (T=120 C, CatLoad=25.7 g_{cat} dm^{-3}) led to comparable catalytic results, with 2BFE as predominant bioP. For a reaction time of 7 h, the highest conversion and total bioP yield (87% and 75%, respectively) were obtained for CatLoad=25.7 g_{cat} dm^{-3} and T=150 C.

As mentioned above, other products of the Fur/2BuOH reaction system included LA and GVL which were formed in low yields. LA and GVL are value-added chemicals reported by the US Department of Energy.[157,158] From Scheme 1 it can be verified that these products are formed further down the cascade reactions of Fur, with GVL as an important end-product. According to the literature, GVL may be formed from LA[155,159,160] or LEs[87,155,156,161] in alcohol media via CTH reaction, in the presence of zirconium-containing catalysts. The catalytic potential of ZrAl-Beta/TUD-1 for GVL production was further investigated using LA and 1-butyl levulinate (1BL) as model substrates (CatLoad=25.7 g_{cat} dm^{-3}, T=150 C, Figures 10 and 11). With LA as substrate, 2BL and GVL were formed with very high total selectivity at high LA conversion, although the reaction was slow (91% total selectivity at 91% LA conversion reached at 72 h). With 1BL, ZrAl-Beta/TUD-1 led to high very GVL selectivity (Figure 11-b), but the reaction was slow (91% selectivity at 59% conversion, 72 h reaction, Figure 10). For the two substrates, a long induction period was observed in the formation of GVL. The kinetic profiles are consistent with a reaction mechanism involving esterification of LA to give the levulinate ester, followed by reduction and lactonization reactions leading to GVL, in agreement with the literature.[87,156,159,161] Based on these results, the low GVL yield for Fur conversion may be partly due to slow conversion of the LA and levulinate ester intermediates. Nevertheless, ZrAl-Beta/TUD-1 with LA as substrate led to much higher 2BL and GVL yields (53% 2BL and 31% GVL yield at 91% LA conversion) than with Fur (14% 2BL and 1% GVL yield at 97% Fur conversion), suggesting that it is a more effective catalyst for carrying out the reaction systems Fur-to-FEs and LA-to-(LEs, GVL) separately.

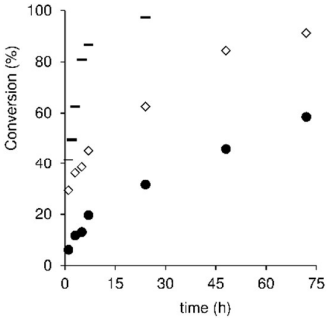

Figure 10 Catalytic performance of ZrAl-Beta/TUD-1 in the reaction of Fur (–), LA (◊) or 1BL (•). Reaction conditions: 0.45 M substrate in 2BuOH, CatLoad=25.7 g_{cat} dm^{-3}, T=150 C.

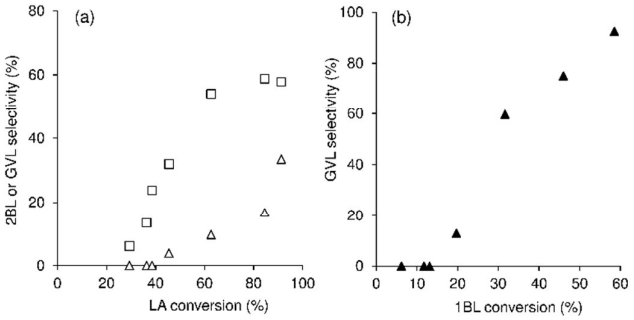

Figure 11 Catalytic performance of ZrAl-Beta/TUD-1 in the reactions of LA and 1BL: (a) dependence of 2BL (□) and GVL (Δ) selectivity on LA conversion; (b) dependence of GVL (Δ) selectivity on 1BL conversion. Reaction conditions: 0.45 M substrate in 2BuOH, CatLoad=25.7 g_{cat} dm^{-3}, T=150 C.

ZrAl-Beta/TUD-1, its individual components, and MP-ZrAl-Beta-m. The catalytic performance of ZrAl-Beta/TUD-1 in the Fur conversion process was compared to those of: (i) bulk mesoporous silica TUD-1 used in an amount equivalent to the mass of the TUD-1 type component added in ZrAl-Beta/TUD-1; (ii) nanocrystalline ZrAl-Beta-n used in an amount equivalent to the mass of zeotype component added in ZrAl-Beta/TUD-1; and (iii) mechanically mixed TUD-1 and ZrAl-Beta-n (denoted ZrAl-Beta-n+TUD-1), used in amounts (total load of 25.7 g dm^{-3}) equivalent to the respective masses added with ZrAl-Beta/TUD-1 (T=150 C, Figures 12 and 13). The mesoporous silica TUD-1 led to 27% Fur conversion and negligible total bioP yield at 24 h reaction, similar to that observed without catalyst (20% conversion). Hence, the active sites of the composite are located in its zeotype component, which is consistent with the acid properties measurements (silica TUD-1 possessed negligible acidity). For bulk ZrAl-Beta-n as catalyst, lower Fur conversion and total bioP yields were reached than for the composite. Hence, the performance of ZrAl-Beta/TUD-1 is superior to that of the individual components. The composite catalyst led to higher total bioP yields at high Fur conversions than the mechanical mixture ZrAl-Beta-n+TUD-1 (Figure 12-a), while the reaction rates were similar (69% and 59% total yield, respectively, at 97% conversion, Figure 11). The embedment of the nanocrystallites in the mesoporous siliceous matrix seems to avoid extensive side reactions at high Fur conversions. The presence of carbonaceous matter (CM) in the used solids was confirmed by thermal analyses. The DSC curves of the used ZrAl-containing catalysts show two exothermic peaks at ca. 370 and 470 C, which were not observed for the fresh catalysts. These exothermic processes were accompanied by mass loss attributed to the decomposition of CM (exemplified in Figure S7-a for ZrAl-Beta/TUD-1). The amount of CM in the used solids followed the order ZrAl-Beta-n (28.5 wt%) >> ZrAl-Beta-n+TUD-1 (16.3 wt%) > ZrAl-Beta/TUD-1 (15.7 wt%). The material balances (considering unconverted Fur, identified products (i.e., FA, 2BFE, 2BL, AnLs, LA, GVL) and the amount of CM) closed in ca. 77-79% for ZrAl-Beta-n and ZrAl-Beta-n+TUD-1, and ca. 86% for ZrAl-Beta/TUD-1; the remaining material likely corresponds to soluble byproducts (the liquid phases of the reaction mixtures were brownish in colour). The greater material balance for ZrAl-Beta/TUD-1 was mainly due to the higher total bioP yield reached with this catalyst.

View Article Online
DOI: 10.1039/C6CY00223D

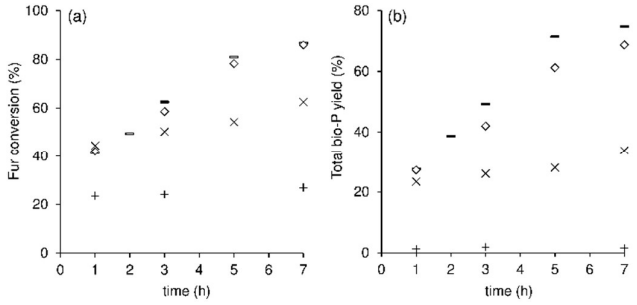

Figure 12 Reaction of Fur in the presence of ZrAl-Beta/TUD-1 (–), ZrAl-Beta-n (×), TUD-1 (+) or ZrAl-Beta-n+TUD-1 (◊); (a) Fur conversion and (b) total bioP yield dependence on reaction time. Reaction conditions: 0.45 M Fur in 2BuOH, T=150 C.

A comparative study for ZrAl-Beta/TUD-1 and ZrAl-Beta-n on the basis of similar mass of catalyst (CatLoad=25.7 g_{cat} dm^{-3}, at 150 C) indicated higher Fur conversions until ca. 3-5 h reaction for the nanocrystalline catalyst (conversion at 3 h was 77% and 63% for ZrAl-Beta-n and ZrAl-Beta/TUD-1, respectively, Figure 14). The initial reaction rate (based on conversion at 1 h reaction) was 7.2 and 12.1 mmol g_{cat}^{-1} h^{-1} for ZrAl-Beta/TUD-1 and ZrAl-Beta-n, respectively, which correlates with the amounts of acid sites (highest for ZrAl-Beta-n, Table 3). However, ZrAl-Beta-n led to a drastic drop of total bioP yield at high Fur conversions; 70%/24% total yield at 85%/98% conversion, compared to 75%/69% total yield at 87%/97% conversion for ZrAl-Beta/TUD-1. The total yield drop for ZrAl-Beta-n was accompanied by a drastic drop of 2BFE yield (61%/4%) (Figure 14-d). The catalytic performance of ZrAl-Beta/TUD-1 compares favourably (based on total bioP yield at ca. 90% Fur conversion) to previously investigated mesoporous bulk silicates of the type TUD-1 possessing framework Zr-sites, or Zr- plus Al-sites, tested as catalysts under similar Fur reaction conditions (T=120 C; catalyst load=25.7 g_{cat} dm^{-3}).[79] ZrAl-Beta/TUD-1 led to a bioP yield (2BFE+2BL+AnLs) of 65% at 89% conversion (Figure S5), which was higher than for the previously reported best-performing mesoporous silicate Zr-TUD-1 (54% yield at 90% conversion).[79] For the two materials, the main reaction products were 2BFE, 2BL and AnLs, with 2BFE being predominant. However, Zr-TUD-1 led to faster Fur reaction than ZrAl-Beta/TUD-1 (ca. 90% conversion was reached at 24 h and 48 h, respectively).[79] These results may be partly associated with the fact that Zr-TUD-1 is a bulk catalyst, whereas ZrAl-Beta/TUD-1 is a composite of ca. 40 wt% ZrAl-Beta-n in a siliceous matrix.

It is desirable to enhance the overall Fur reaction rate and obtain high bioP yields. Mechanical mixtures of ZrAl-Beta/TUD-1 and H-Beta-n, or of bulk ZrAl-Beta-n and H-Beta-n (enhancing contribution of Al-sites in the reaction system) did not improve the catalytic results (Table S1). Alternatively, a bulk catalyst possessing simultaneously BEA topology and mesoporosity, namely MP-ZrAl-Beta-m, was prepared and explored for Fur conversion (CatLoad=25.7 g_{cat} dm^{-3}; T=150 C, Figure 14). MP-ZrAl-Beta-m led to very high total bioP yield at high Fur conversion, and excellent selectivity towards 2BFE (95% total bioP yield, and 88% 2BFE yield at 99% Fur conversion, reached at 5 h reaction). The Zr-free synthetic precursors of MP-ZrAl-Beta-m, namely H-Beta-m, OxAc-Beta-m, MP-Beta-m and deAl-MP-Beta-m, led to sluggish Fur reaction (less than 8% bioP yield, 12-38% conversion at 24 h, Table S2), demonstrating the importance of the Zr-sites of MP-ZrAl-Beta-m for Fur reaction. The used catalyst (after 99% Fur conversion was reached) possessed relatively low amount of CM (ca. 7 wt.% based on TGA, Figure S7-b).

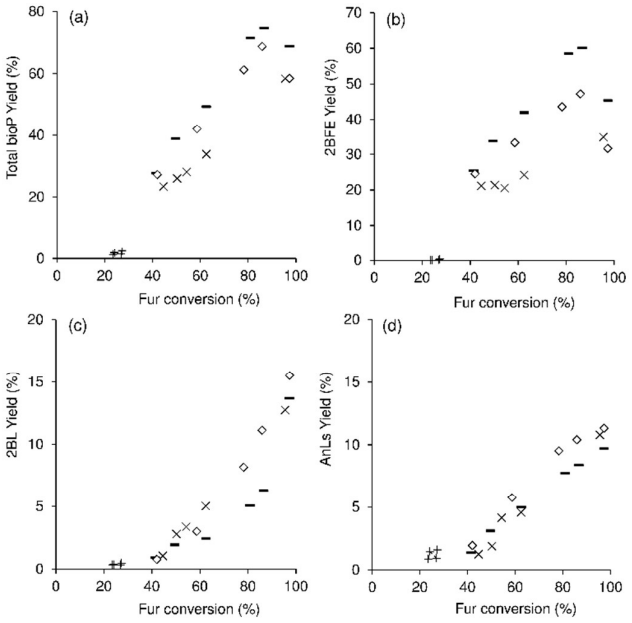

Figure 13 Reaction of Fur in the presence of (–) ZrAl-Beta/TUD-1, (×) ZrAl-Beta-n, (+) TUD-1 or (◊) ZrAl-Beta-n+TUD-1; (a) total bioP yield, (b) 2BFE yield, (c) 2BL yield, and (d) AnLs yield dependence on Fur conversion. Reaction conditions: 0.45 M Fur in 2BuOH, T=150 C.

The establishment of structure-activity relationships for materials of different types is difficult due to the significant number of possible variables. Nevertheless, it is interesting that MP-ZrAl-Beta-m seems to perform superior to ZrAl-Beta/TUD-1 and ZrAl-Beta-n (Figure 14). A comparative study for the bulk catalysts MP-ZrAl-Beta-m and ZrAl-Beta-n indicates that the latter led to faster initial reaction rate (10.0 and 12.2 mmol g_{cat}^{-1} h^{-1}, respectively). Nevertheless, for nanocrystalline ZrAl-Beta-n, Fur reaction slowed down considerably (Figure 14- and ZrAl-Beta-n a), possibly due to significant catalyst surface passivation by CM. The faster reaction for ZrAl-Beta-n than MP-ZrAl-Beta-m correlates with the higher amounts of acid sites of the former. As discussed above, Zr-sites are important for triggering the Fur reaction. Hence, the higher initial activity of ZrAl-Beta-n may be due to the higher amount of Zr-sites (i.e. lower Si/(Zr+Al) ratio and higher Zr/Al ratio, Table 1), or higher amount of L acid sites (L acidity is essentially associated with the Zr-sites, discussed in section 3.1, Table 3). On the other hand, MP-ZrAl-Beta-m possesses a slightly higher Si/(Zr+Al) molar ratio (Table 1) and slightly lower amounts of acid sites (Table 3) than ZrAl-Beta/TUD-1, even though the former led to faster initial reaction of Fur (10.0 and 7.2 mmol g_{cat}^{-1} h^{-1}, respectively), Figure 14-a. These results suggest that the amount of acid sites is not the sole factor responsible for the catalytic reaction.

Based on turnover frequency (TOF, expressed as mol mol_L^{-1} h^{-1}, where L is the amount of Lewis acid sites), MP-ZrAl-Beta-m seems to possess Lewis acid (Zr) sites with higher intrinsic activity (137 mol mol_L^{-1} h^{-1}) than ZrAl-Beta-n and ZrAl-Beta/TUD-1 (115 and 92 mol

View Article Online
DOI: 10.1039/C6CY00223D

mol_L^{-1} h^{-1}, respectively) for Fur conversion. The higher intrinsic activity for MP-ZrAl-Beta-m does not seem to be due to differences in L acid strength, since the three materials possessed similar acid strengths (ascertained by FT-IR of adsorbed pyridine). The catalytic activity possibly results from interplay of acid and texture properties, and active sites accessibility may be more favourable for the best performing catalyst MP-ZrAl-Beta-m. For MP-ZrAl-Beta-m and ZrAl-Beta-n, molecules diffusing inside the channels may access active sites dispersed in the whole bulk; for ZrAl-Beta/TUD-1, the embedded active component is likely accessed through the mesoporous channels (matrix), and some sites may be hardly accessible at contacting regions between the two components.

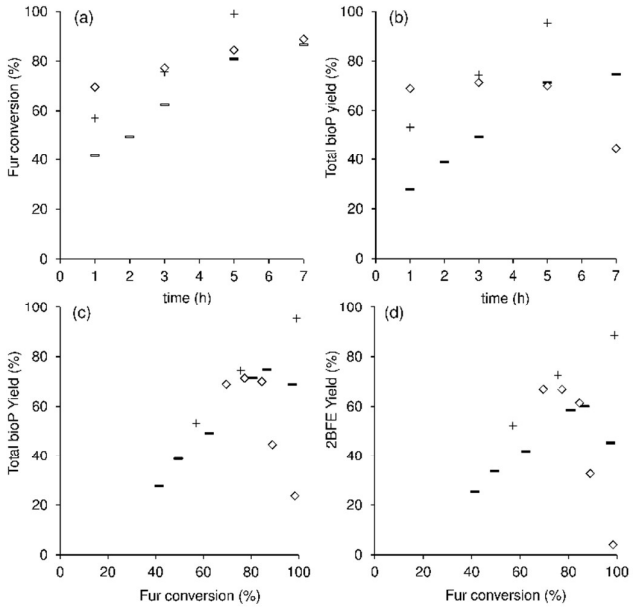

Figure 14 Fur/2BuOH reaction in the presence of (-) ZrAl-Beta/TUD-1, (◊) ZrAl-Beta-n, or (+) MP-ZrAl-Beta-m; (a) dependence of Fur conversion and (b) total bioP yield on reaction time, and (c) dependence of total bioP yield and (d) 2BFE yield on Fur conversion. Reaction conditions: 0.45 M Fur, CatLoad=25.7 gcat dm-3, T=150 C.

Catalytic stability. The catalyst stabilities of ZrAl-Beta/TUD-1 and MP-ZrAl-Beta-m were investigated by reusing the recovered solids in consecutive batch runs (details given in the experimental section; T=150 C, CatLoad=25.7 g_{cat} dm^{-3}, Figure 15). For ZrAl-Beta/TUD-1, the Fur conversions and total bioP yields in three consecutive runs were in the range 97-100% and 62-69%, respectively. The somewhat steady catalytic performance of ZrAl-Beta/TUD-1 correlated with the similar characterisation results for the fresh and spent catalysts. Specifically, the composite catalyst preserved its structural features (PXRD, Figure 1-a, Figure S1), compositions (ICP-AES, Table 1), textural properties (Table 2, Figure 4-a), and chemical characteristics (FT-IR (Figure 5-a), DR UV-vis (Figure S4-a), and ^{27}Al MAS NMR (Figure 7-a)). SEM revealed no obvious changes with respect to morphology or elemental distribution maps. The recyclability of ZrAl-Beta/TUD-1 was investigated in a similar fashion for the LA/2BuOH reaction system (Figure S8); no drop of LA conversion was observed for three consecutive 24 h-batch runs, and the total yields of 2BL plus GVL remained similar (conversion tended to increase slightly, and the GVL/2BL molar ratio increased slightly from run 1 to run 2). Good catalyst stability was also observed for bulk MP-ZrAl-Beta-m, and the steady performance in consecutive batch runs correlated with the similar characterisation results for the original and used solids, i.e. they possessed comparable structural features (PXRD, Figure 1-b), compositions (Table 1), textural properties (Table 2, Figure 4-b), and chemical characteristics (FT-IR (Figure 5-b), DR UV-vis (Figure S4-b) and ^{27}Al MAS NMR (Figure 7-b)).

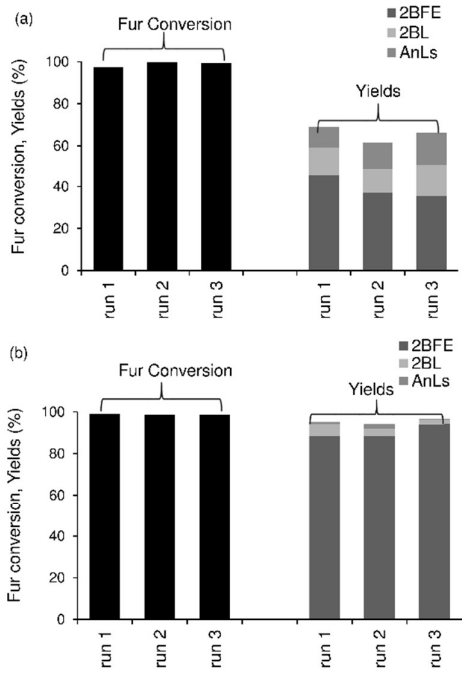

Figure 15 Fur conversion and bioP yields for consecutive batch runs using (a) the composite catalyst ZrAl-Beta/TUD-1 and (b) MP-ZrAl-Beta-m. Reaction conditions: 0.45 M Fur in 2BuOH, T=150 C, CatLoad=25.7 g_{cat} dm^{-3}.

Conclusions

Zeolites can be modified via different synthetic strategies making them promising catalysts for the valorization of furfural (Fur), an industrially produced renewable platform chemical. Bulk and composite catalysts, each combining BEA topology, mesoporosity and framework Zr- and Al-sites, were prepared and explored for the integrated reduction/acid reaction of Fur to useful bio-products (bioP), namely furanic ethers, levulinate esters and angelica lactones, in alcohol media at 120-150 C.

The different synthetic strategies started with pre-formed nanocrystalline or microcrystalline zeolite Beta. Pre-formed microcrystalline H-Beta-m was subjected to a series of treatments involving desilication to introduce mesoporosity, partial dealumination and SSIE to introduce Zr-sites, leading to a bulk zeotype possessing mesoporosity (MP-ZrAl-Beta-m) On the other hand, Zr,Al-containing Beta type nanocrystallites (formed from zeolite nanocrystals via dealumination and SSIE for Zr) were embedded in a mesoporous siliceous matrix of the type TUD-1 giving a composite material (ZrAl-Beta/TUD-1). The prepared catalysts led to high bioP yield at high Fur conversion, and the

View Article Online
DOI: 10.1039/C6CY00223D

predominant bioP of the Fur/2-butanol reaction system was 2-butyl furfuryl ether (2BFE). Up to 93% total bioP yield at 96% Fur conversion was reached for the composite catalyst ZrAl-Beta/TUD-1, and it performed superior to its individual components. The composite was also capable of promoting (i) the conversion of levulinic acid (as substrate) to levulinate ester and γ-valerolactone (GVL) which were formed with a total selectivity of 91% at 91% LA conversion, as well as (ii) the conversion of levulinate ester to GVL (91% selectivity at 59% 1-butyl levulinate conversion). The bulk catalyst MP-ZrAl-Beta-m led to a total bioP yield of 95% at 99% Fur conversion, and 2BFE was formed in a high yield of 89% yield at 5 h reaction, 150 °C. The catalytic results correlated with the compositions and amounts of acid sites for the bulk catalysts MP-ZrAl-Beta-m and ZrAl-Beta-n. However, this factor did not solely explain the superior performance of MP-ZrAl-Beta-m in relation to the composite, which may be due to favourable interplay of acid and texture properties.

Catalyst recycling and detailed structural characterisation of the spent catalysts indicated fairly good stabilities for ZrAl-Beta/TUD-1 and MP-ZrAl-Beta-m. These types of materials are promising catalysts with tuneable properties for different integrated reduction/acid reaction systems.

Acknowledgements

This work was developed within the scope of the project CICECO-Aveiro Institute of Materials, POCI-01-0145-FEDER-007679 (FCT Ref. UID /CTM /50011/2013), financed by national funds through the FCT/MEC and when appropriate co-financed by FEDER under the PT2020 Partnership Agreement. The FCT and the European Union are acknowledged for grants to M.M.A. (SFRH/BPD/89068/2012), P.N. (SFRH/BPD/73540/2010), A.F.S (SFRH/BD/101018/2014) and A.F. (SFRH/BPD/91397/2012), cofunded by MCTES and the ESF through the program POPH of QREN. The authors thank Vânia Freitas for support with DR UV-vis spectroscopy measurements.

References

1 P. T. Anastas and J. C. Warner, Green Chemistry Pocket Guides, http://www.acs.org/content/acs/en/greenchemistry/what-is-green-chemistry/principles/green-chemistry-pocket-guides.html (accessed 16 th December 2015, 2015).
2 J. N. Chheda, G. W. Huber and J. A. Dumesic, *Angew. Chem. Int. Ed.*, 2007, **46**, 7164.
3 Y.-C. Lin and G. W. Huber, *Energy Environ. Sci.*, 2009, **2**, 68.
4 M. J. Climent, A. Corma and S. Iborra, *Green Chem.*, 2014, **16**, 516.
5 A. Wang, C. Li, M. Zheng and T. Zhang, *The Role of Green Chemistry in Biomass Processing and Conversion*, eds. H. Xie and N. Gathergood, John Wiley & Sons, Inc., Hoboken, New Jersey, 2013, chapter 11, pp. 313-345.
6 J. Weitkamp, *Solid State Ionics*, 2000, **131**, 175.
7 G. W. Huber, S. Iborra and A. Corma, *Chem. Rev*, 2006, **106**, 4044.
8 M. I. Alam and B. Saha, *Sustainable Catalytic Processes*, eds. B. Saha, M. Fan and J. Wang, Elsevier B. V., Amsterdam, Boston, Heidelberg, London, New York, Oxford, Paris, San Diego, San Franciso, Singapore, Sydney, Tokyo, 2015, chapter 4, pp. 99-123.
9 D. Kubička and O. Kikhtyanin, *Catal. Today*, 2015, **243**, 10.
10 T. Suzuki and T. Okuhara, *Micropor. Mesopor. Mat.*, 2001, **43**, 83.
11 M. Ogura, S. Y. Shinomiya, J. Tateno, Y. Nara and E. Kikuchi, *Chem. Lett.*, 2000, **8**, 882.
12 J. C. Groen, L. A. A. Peffer, J. A. Moulijn, J. Pérez-Ramírez, *Micropor. Mesopor. Mat.*, 2004, **69**, 29.
13 M. Ogura, S. Shinomiya, J. Tateno, Y. Nara, M. Nomura, E. Kikuchi, M. Matsukata, *Appl. Catal. A- Gen.*, 2001, **219**, 33-44.
14 J. C. Groen, J. Pérez-Ramırez and L. A. A. Peffer, *Chem. Lett.*, 2002, **31**, 94.
15 J. Pérez-Ramírez, C. H. Christensen, K. Egeblad, C. H. Christensen and J. C. Groen, *Chem. Soc. Rev.*, 2008, **37**, 2530.
16 R. Chal, C. Gérardin, M. Bulut and S. van Donk, *ChemCatChem*, 2011, **3**, 67.
17 S. Lopez-Orozco, A. Inayat, A. Schwab, T. Selvam and W. Schwieger, *Adv. Mater.*, 2011, **23**, 2602.
18 J. Li, X. Li, G. Zhou, W. Wang, C. Wang, S. Komarneni and Y. Wang, *Appl. Catal. A- Gen.*, 2014, **470**, 115.
19 H. Wang, J. Lv, X. Zhu, X. Liu, J. Han and Q. Ge, *Top Catal.*, 2015, **58**, 623.
20 K. Y. Nandiwale, N. D. Galande, P. Thakur, S. D. Sawant, V. P. Zambre and V. V. Bokade, *ACS Sustain. Chem. Eng.*, 2014, **2**, 1928.
21 V. Rac, V. Rakić, D. Stošić, O. Otman and A. Auroux, *Micropor. Mesopor. Mat.*, 2014, **194**, 126.
22 B. Chamnankid, C. Ratanatawanate and K. Faungnawakij, *Chem. Eng. J.*, 2014, **258**, 341.
23 S. J. You and E. D. Park, *Micropor. Mesopor. Mat.*, 2014, **186**, 121.
24 K. Y. Nandiwale, A. M. Pande and V. V. Bokade, *RSC Adv.*, 2015, **5**, 79224.
25 K. Y. Nandiwale and V. V. Bokade, *Environ. Progr. Sustain. Energy*, 2015, **34**, 795.
26 C. R. Patil, P. S. Niphadkar, V. V. Bokade and P. N. Joshi, *Catal. Commun.,* 2014, **43**, 1881.
27 P. Y. Dapsens, C. Mondelli and J. Pérez-Ramírez, *ChemSusChem*, 2013, **6**, 831.
28 J. Xing, L. Song, C. Zhang, M. Zhou, L. Yue and X. Li, *Catal. Today*, 2015, **258,** Part 1, 90.
29 S. Stefanidis, K. Kalogiannis, E. F. Iliopoulou, A. A. Lappas, J. M. Triguero, M. T. Navarro, A. Chica and F. Rey, *Green Chem.*, 2013, **15**, 1647.
30 P. Y. Dapsens, C. Mondelli and J. Perez-Ramirez, *New J. Chem.*, 2016, DOI: 10.1039/C5NJ01834J, 10.1039/C1035NJ01834J.
31 L. Yunqi, C. Liu and L. Chenguang, *Prog. Chem.*, 2005, **17**, 666.
32 A. Molenbroek, S. Helveg, H. Topsøe and B. Clausen, *Top Catal.*, 2009, **52**, 1303.
33 S. Chaturvedi, P. N. Dave and N. K. Shah, *J. Saudi Chem. Soc.*, 2012, **16**, 307.
34 H. Wu, A. Duan, Z. Zhao, T. Li, R. Prins and X. Zhou, *J. Catal.*, 2014, **317**, 303.
35 Y. Sang, Q. Jiao, H. Li, Q. Wu, Y. Zhao and K. Sun, *J. Nanopart Res*, 2014, **16**, 1.
36 C. Buzea, I. L. P. Blandino and K. Robbie, *Biointerphases*, 2007, **2**, MR17.
37 J. C. Jansen, Z. Shan, L. Marchese, W. Zhou, N. v. d. Puil and T. Maschmeyer, *Chem. Commun.*, 2001, 713.
38 P. Waller, Z. Shan, L. Marchese, G. Tartaglione, W. Zhou, J. C. Jansen and T. Maschmeyer, *Chem. Eur. J.*, 2004, **10**, 4970.
39 Y. Xia and R. Mokaya, *J. Mat. Chem.*, 2004, **14**, 863.
40 V. Mavrodinova, M. Popova, V. Valchev, R. Nickolov and C. Minchev, *J. Colloid Interf Sci.*, 2005, **286**, 268.
41 N. Petkov, M. Hölzl, T. H. Metzger, S. Mintova and T. Bein, *J. Phys. Chem. B*, 2005, **109**, 4485.
42 Z. Shan, P. W. G. Waller, B. G. Maingay, P. J. Angevine, J. C. Jansen, C. Y. Yeh, T. Maschmeyer, F. M. Dautzenberg, L. Marchese and H. de O. Pastore, *US 7084087 B2 Pat.,* 2006.

View Article Online
DOI: 10.1039/C6CY00223D

43 I. I. Ivanova, E. E. Knyazeva, A. A. Maerle and I. A. Kasyanov, *Kinet. Catal.*, 2015, **56**, 549.
44. S. Lima, M. M. Antunes, A. Fernandes, M. Pillinger, M. F. Ribeiro and A. A. Valente, *Appl. Catal. A- Gen.*, 2010, **388**, 141.
45 Z. Shan, W. Zhou, J. C. Jansen, C. Y. Yeh, J. H. Koegler and T. Maschmeyer, *Stud. Surf. Sci. Catal.*, 2002, **141**, 635.
46 P. Neves, S. Lima, M. Pillinger, S. M. Rocha, J. Rocha and A. A. Valente, *Catal. Today*, 2013, **218–219**, 76.
47 H. Xu, J. Guan, S. Wu and Q. Kan, *J. Colloid Interf. Sci.*, 2009, **329**, 346.
48 V. L. Struzhko, P. S. Yaremov, E. V. Senchylo, V. M. Solomakha and V. G. Ilyin, *Theor. Exp. Chem.*, 2014, **50**, 323.
49 P. Prokešová, N. Žilková, S. Mintova, T. Bein and J. Čejka, *Appl. Catal. A-Gen.*, 2005, **281**, 85.
50 P. Prokešová, S. Mintova, J. Čejka and T. Bein, *Mater. Sci. Eng. C*, 2003, **23**, 1001.
51 A. Duan, C. Wang, Z. Zhao, Z. Tong, T. Li, H. Wu, H. Fan, G. Jiang and J. Liu, *J. Porous Mat.*, 2013, **20**, 1195.
52 P. Prokešová-Fojtíková, S. Mintova, J. Čejka, N. Žilková and A. Zukal, *Micropor. Mesopor. Mat.*, 2006, **92**, 154.
53 D. Gao, A. Duan, X. Zhang, K. Chi, Z. Zhao, J. Li, Y. Qin, X. Wang and C. Xu, *J. Mater. Chem. A*, 2015, **3**, 16501.
54 Y. Lv, X. Qian, B. Tu and D. Zhao, *Catal. Today*, 2013, **204**, 2.
55 M. S. Hamdy and G. Mul, *ChemCatChem*, 2013, **5**, 3156.
56 Q. Tan, X. Bao, T. Song, Y. Fan, G. Shi, B. Shen, C. Liu and X. Gao, *J. Catal.*, 2007, **251**, 69.
57 A. Duan, T. Li, Z. Zhao, B. Liu, X. Zhou, G. Jiang, J. Liu, Y. Wei and H. Pan, *Appl. Catal. B: Environ*, 2015, **165**, 763.
58 T. Li, A. Duan, Z. Zhao, B. Liu, G. Jiang, J. Liu, Y. Wei and H. Pan, *Fuel*, 2014, **117,** Part B, 974.
59 Q. Huo, Y. Gong, T. Dou, Z. Zhao, H. Pan and F. Deng, *Energ Fuel*, 2010, **24**, 3764.
60 H. Yu, Y. Lv, K. Ma, C. Wang, Z. Xue, Y. Zhao, Y. Deng, Y. Dai and D. Zhao, *J. Colloid Interface Sci.*, 2014, **428**, 251.
61 J. Zhou, H. Zhao, J. Li, Y. Zhu, J. Hu, H. Liu and Y. Hu, *Solid State Sciences*, 2013, **24**, 107-114.
62 L. Huang, W. Guo, P. Deng, Z. Xue and Q. Li, *J. Phys. Chem. B*, 2000, **104**, 2817.
63 Q. Tang, H. Xu, Y. Zheng, J. Wang, H. Li and J. Zhang, *Appl. Catal. A- Gen.*, 2012, **413–414**, 36.
64 C. Huiyong, X. Hongxia, C. Xianying and Q. Yu, *Micropor. Mesopor. Mat.*, 2009, **118**, 396.
65 C.-M. Song, J. Jiang and Z.-F. Yan, *J. Porous Mat.*, 2008, **15**, 205.
66 Y. Sang, H. Liu, S. He, H. Li, Q. Jiao, Q. Wu and K. Sun, *J. Energy Chem.*, 2013, **22**, 769.
67 D. P. Serrano, R. A. García, G. Vicente, M. Linares, D. Procházková and J. Čejka, *J.Catal.*, 2011, **279**, 366.
68 H. Li, S. He, K. Ma, Q. Wu, Q. Jiao and K. Sun, *Appl. Catal. A-Gen.*, 2013, **450**, 152.
69 M. Kollár, R. M. Mihályi, G. Pál-Borbély and J. Valyon, *Micropor. Mesopor. Mat.*, 2007, **99**, 37.
70 J. Qi, Q. Jin, K. Zhao and T. Zhao, *J. Porous Mat.*, 2015, **22**, 1021.
71 J. Qi, T. Zhao, X. Xu, F. Li and G. Sun, *Sci. China Chem.*, 2010, **53**, 2279.
72 Y. Zhu, T. E. Müller and J. A. Lercher, *Adv. Funct. Mater.*, 2008, **18**, 3427
73 J. Zhou, Z. Hua, J. Shi, Q. He, L. Guo and M. Ruan, *Chem- Eur. J.*, 2009, **15**, 12949.
74 C. C. Aquino , H. O. Pastore, A. F. Masters and T. Maschmeyer, *ChemCatChem*, 2011, **3**, 1759.
75 D. T. Win, *Au J. T.*, 2005, **8**, 185.
76 K. J. Zeitsch, *The Chemistry and Technology of Furfural and Its Many By-Products*, Elsevier, The Netherlands, 2000.
77 J. B. Joseph, *Feedstocks for the Future*, American Chemical Society, 2006, vol. 921, chapter 1, pp. 1-12.
78 L. Bui, H. Luo, W. R. Gunther and Y. Román-Leshkov, *Angew.Chemie Int. Ed.*, 2013, **52**, 8022.
79 M. M. Antunes, S. Lima, P. Neves, A. L. Magalhães, E. Fazio, F. Neri, M. T. Pereira, A. F. Silva, C. M. Silva, S. M. Rocha, M. Pillinger, A. Urakawa and A. A. Valente, *Appl. Catal. B: Environ.*, 2016, **182**, 485.
80 A. B. Kellicutt, R. Salary, O. A. Abdelrahman and J. Q. Bond, *Cat. Sci.Tec.*, 2014, **4**, 2267.
81 R. J. Haan, J.-P. Lange, *US 8372164 B2 Pat.,* 2013.
82 B. Vanderhaegen, H. Neven, L. Daenen, K. J. Verstrepen, H. Verachtert and G. Derdelinckx, *J. Agric. Food Chem.,* 2004, **52**, 1661.
83 H. Joshi, B. R. Moser, J. Toler, W. F. Smith and T. Walker, *Biomass Bioenerg.*, 2011, **35**, 3262.
84 U. Addepally and C. Thulluri, *Fuel*, 2015, **159**, 935.
85. L. E. Manzer, *WO 097724 A1 Pat.,* 2005.
86. L. Lomba, B. Giner, I. Bandres, C. Lafuente and M. R. Pino, *Green Chem.*, 2011, **13**, 2062.
87 A. Démolis, N. Essayem and F. Rataboul, *ACS Sustain. Chem. Eng.*, 2014, **2**, 1338.
88 H. J. Bart, J. Reidetschlager, K. Schatka and A. Lehmann, *Ind. Eng. Chem. Res.*, 1994, **33**, 21.
89 Yom-Tov, *EP 1833790 B1 Pat.,* 2011.
90 R. Cao, J. Xin, Z. Zhang, Z. Liu, X. Lu, B. Ren and S. Zhang, *ACS Sustain. Chem. Eng.*, 2014, **2**, 902.
91 J. Cardellach, J. Font and R. M. Ortuño, *J. Heterocyclic Chem.*, 1984, **21**, 327.
92 D. C. Elliot, J. G. Frye, *US 5883266 Pat.,* 1999.
93 M. M. Antunes, S. Lima, P. Neves, A. L. Magalhães, E. Fazio, A. Fernandes, F. Neri, C. M. Silva, S. M. Rocha, M. F. Ribeiro, M. Pillinger, A. Urakawa and A. A. Valente, *J. Catal.*, 2015, **329**, 522.
94 C. Hammond, S. Conrad and I. Hermans, *Angew. Chemie Int. Ed.*, 2012, **51**, 11736.
95 S. Telalovi, A. Ramanathan, G. Mul and U. Hanefeld, *J. Mater. Chem.*, 2010, **20**, 642.
96 R. Anand, R. Maheswari and U. Hanefeld, *J. Catal.*, 2006, **242**, 82.
97 R. Anand, M. S. Hamdy, P. Gkourgkoulas, T. Maschmeyer, J. C. Jansen and U. Hanefeld, *Catal. Today*, 2006, **117**, 279.
98 M. S. Hamdy, A. Ramanathan, T. Maschmeyer, U. Hanefeld and J. C. Jansen, *Chem.- Eur. J.*, 2006, **12**, 1782.
99 A. Ramanathan, M. C. Castro Villalobos, C. Kwakernaak, S. Telalovic and U. Hanefeld, *Chem.-Eur. J.*, 2008, **14**, 961.
100 J. ten Dam, D. Badloe, A. Ramanathan, K. Djanashvili, F. Kapteijn and U. Hanefeld, *Appl. Catal. A- Gen.*, 2013, **468**, 150.
101 W. Tanglumlert, S.-T. Yang, K.-E. Jeong, S.-Y. Jeong and W.-S. Ahn, *Res Chem Intermed*, 2011, **37**, 1267.
102 H. Maneesuwan, S. Tantisriyanurak, T. Chaisuwan and S. Wongkasemjit, *Appl. Catal. A-Gen.*, 2015, **504**, 448.
103 S. Mandal, A. SinhaMahapatra, B. Rakesh, R. Kumar, A. Panda and B. Chowdhury, *Catal. Commun.*, 2011, **12**, 734.
104 S. Rahman, S. A. Farooqui, A. Rai, R. Kumar, C. Santra, V. C. Prabhakaran, G. R. Bhadu, D. Sen, S. Mazumder, S. Maity, A. K. Sinha and B. Chowdhury, *RSC Adv.*, 2015, **5**, 46850.
105 S. Mandal, S. Rahman, R. Kumar, K. K. Bando and B. Chowdhury, *Catal. Commun.*, 2014, **46**, 123.
106 B. Tang, W. Dai, X. Sun, G. Wu, N. Guan, M. Hunger and L. Li, *Green Chem.*, 2015, **17**, 1744.
107 J. C. Groen, J. C. Jansen, J. A. Moulijn and J. Pérez-Ramírez, *J. Phys. Chem. B*, 2004, **108**, 13062.
108 M. A. Camblor, A. Corma and S. Valencia, *J. Mater. Chem.*, 1998, **8**, 2137.
109 J. Yu, *Studies in Surface Science and Catalysis, Introduction to Zeolite Science and Practice*, eds. J. Čejka, H. v. Bekkum, A. Corma and F. Schueth, Elsevier, Amesterdam, the Netherlands, 3 rd edn., 2007, vol. 168, chapter 3, pp. 39-103.
110 E. M. Flanegen, R. L. Patton, *US 4073865 Pat.,* 1978.
111 S. Morin, P. Ayrault, N. S. Gnep, M. Guisnet, *Appl. Catal. A-Gen.*,1998, **166**, 281.

View Article Online
DOI: 10.1039/C6CY00223D

112 A. Simon-Masseron, J. P. Marques, J. M. Lopes, F. R. Ribeiro, I. Gener and M. Guisnet, *Appl. Catal. A- Gen.*, 2007, **316**, 75.
113 I. Kiricsi, C. Flego, G. Pazzuconi, W. O. Parker, Jr., R. Millini, C. Perego and G. Bellussi, *J. Phys. Chem.*, 1994, **98**, 4627.
114 C. Li and Z. Wu, *Handbook of Zeolite Sicence and Technology*, eds. S. M. Auerbach, K. A. Carrado and P. K. Dutta, Marcel Dekker, Inc., Basel, Switzerland, 2003, chapter 11.
115 S. Lima, M. M. Antunes, A. Fernandes, M. Pillinger, M. F. Ribeiro and A. A. Valente, *Molecules*, 2010, **15**, 3863.
116 S. Telalović, A. Ramanathan, J. F. Ng, R. Maheswari, C. Kwakernaak, F. Soulimani, H. C. Brouwer, G. K. Chuah, B. M. Weckhuysen and U. Hanefeld, *Chem.-Eur. J.,* 2011, **17**, 2077.
117 C. Simons, U. Hanefeld, I. W. C. E. Arends, R. A. Sheldon and T. Maschmeyer, *Chem.-Eur. J.*, 2004, **10**, 5829.
118 S. Telalović and U. Hanefeld, *Appl. Catal. A- Gen.,* 2010, **372**, 217.
119 K. Byrappa and B. V. S. Kumar, *Asian J. Chem.*, 2007, **19**, 4933.
120 K. Shanjiao, G. Yanjun, D. Tao, Z. Ying and Z. Yanying, *Pet. Sci.*, 2007, **4**, 70.
121 J. M. Newsam, M. M. J. Treacy, W. T. Koetsier and C. B. D. Gruyter, *P. Roy. Soc. Lond. A Mat.*, 1988, **420**, 375.
122 H. G. Karge, *Verified Syntheses of Zeolitic Materials*, ed. H. Robson, Elsevier Science B. V., Amesterdam, The Netherlands, 2001, pp. 69-71.
123 F. Tian, Y. Wu, Q. Shen, X. Li, Y. Chen and C. Meng, *Micropor. Mesopor. Mat.*, 2013, **173**, 129.
124 V. L. Sushkevich, A. Vimont, A. Travert, I. I. Ivanova, *Phys. Chem. C*, 2015, **119**, 17633.
125 M. Boronat, P. Concepción, A. Corma, M. Renz, S. Valencia, *J. Catal*., 2005, **234**, 111.
126 M. Boronat, P. Concepción, A. Corma, M. T. Navarro, M. Renz, S. Valencia, *Phys. Chem. Chem. Phys*., 2009, **11**, 2876.
127 J. Dijkmans, M. Dusselier, D. Gabriëls, K. Houthoofd, P. C. M. M. Magusin, S. Huang, Y. Pontikes, M. Trekels, A. Vantomme, L. Giebeler, S. Oswald, B. F. Sels, *ACS Catal*., 2015, **5**, 928.
128 J. A. van Bokhoven, D. C. Koningsberger, P. Kunkeler, H. van Bekkum and A. P. M. Kentgens, *J. Am. Chem. Soc.*, 2000, **122**, 12842.
129 A. J. Marchi and G. F. Froment, *Appl. Catal.*, 1991, **71**, 139.
130 A. Omegna, M. Vasic, J. Anton van Bokhoven, G. Pirngruber and R. Prins, *Phys. Chem. Chem. Phys*., 2004, **6**, 447.
131 K. A. Bokhoven and N. Danilina, *Zeolites and Catalysis: Synthesis, Reactions and Applications*, eds. J. Čejka, A. Corma and S. Zones, Wile-VCH Verlag GmbH & Co. KGaA, Weinheim, Germany, 2010, vol. 1, chapter 10, pp. 283-300.
132 P. J. Kunkeler, B. J. Zuurdeeg, J. C. van der Waal, J. A. van Bokhoven, D. C. Koningsberger and H. van Bekkum, *J. Catal.*, 1998, **180**, 234.
133 S. Mintova, V. Valtchev, T. Onfroy, C. Marichal, H. Knözinger and T. Bein, *Micropor. Mesopor. Mat.*, 2006, **90**, 237.
134 H. Y. Luo, D. F. Consoli, W. R. Gunther, Y. Román-Leshkov, *J. Catal.*, 2014, **320**, 198.
135 M. Boronat, A. Corma, M. Renz, *J. Phys. Chem. B*, 2006, **110**, 21168.
136 V. L. Sushkevich, D. Palagin, I. I. Ivanova, *ACS Catal.*, 2015, **5**, 4833.
137 R. S. Assary, L. A. Curtiss and J. A. Dumesic, *ACS Catal.*, 2013, **3**, 2694.
138 J. C. Groen, S. Abelló, L. A. Villaescusa and J. Pérez-Ramírez, *Micropor. Mesopor. Mat.*, 2008, **114**, 93.
139 K. Tarach, K. Góra-Marek, J. Tekla, K. Brylewska, J. Datka, K. Mlekodaj, W. Makowski, M. C. I. López, J. M. Triguero and F. Rey, *J. Catal.*, 2014, **312**, 46.
140 M. R. Apelian, A. S. Fung, G. J. Kennedy and T. F. Degnan, *J. Phys. Chem.*, 1996, **100**, 16577.
141 M. A. Camblor, A. Corma and S. Valencia, *Chem. Commun.,* 1996, 2365.
142 K. Cheng, J. Kang, S. Huang, Z. You, Q. Zhang, J. Ding, W. Hua, Y. Lou, W. Deng and Y. Wang, *ACS Catal.*, 2012, **2**, 441.
143 D. Verboekend, G. Vilé and J. Pérez-Ramírez, *Cryst. Growth Des.*, 2012, **12**, 3123.
144 Q. H. Xia, S. C. Shen, J. Song, S. Kawi and K. Hidajat, *J. Catal.*, 2003, **219**, 74.
145 D. P. Serrano, R. Van Grieken, P. Sánchez, R. Sanz and L. Rodrıguez, *Micropor. Mesopor. Mat.*, 2001, **46**, 35.
146 J. Pérez-Ramírez, S. Abelló, A. Bonilla and J. C. Groen, *Adv. Funct. Mater.*, 2009, **19**, 164.
147 Y. Wu, F. Tian, J. Liu, D. Song, C. Jia and Y. Chen, *Micropor. Mesopor. Mat.*, 2012, **162**, 168.
148 A. N. C. van laak, L. Zhang, A. N. Parvulescu, P. C. A. Bruijnincx, B. M. Weckhuysen, K. P. de Jong and P. E. de Jongh, *Catal. Today*, 2011, **168**, 48.
149 J. Perez-Pariente, J. A. Martens and P. A. Jacobs, *Appl. Catal.*, 1987, **31**, 35.
150 M. A. Camblor, A. Corma, A. Mifsud, J. Pérez-Pariente and S. Valencia, *Progress in Zeolites and Microporous Materials, Preceedings of the 11th International Zeolite Conference*, eds. H. Chon, S.-K. Ihm and Y. S. Uh, Elsevier, Seoul, Korea, 1997, vol. 105, pp. 341-348.
151 G. Lietz, K. H. Schnabel, C. Peuker, T. Gross, W. Storek and J. Volter, *J. Catal.*, 1994, **148**, 562.
152 T. Pasini, A. Lolli, S. Albonetti, F. Cavani and M. Mella, *J. Catal.*, 2014, **317**, 206.
153 P. Panagiotopoulou, N. Martin and D. G. Vlachos, *J. Mol. Catal. A: Chem.*, 2014, **392**, 223.
154 P. Panagiotopoulou and D. G. Vlachos, *Appl. Catal. A-Gen.*, 2014, **480**, 17.
155 M. Chia and J. A. Dumesic, *Chem. Commun.*, 2011, **47**, 12233.
156 X. Tang, H. Chen, L. Hu, W. Hao, Y. Sun, X. Zeng, L. Lin and S. Liu, *Appl. Catal. B: Environ.*, 2014, **147**, 827.
157 J. J. Bozell and G. R. Petersen, *Green Chem.*, 2010, **12**, 539.
158 T. Werpy and G. Petersen, *Top Value Added Chemicals from Biomass- Results of Screening for Potential Candidates from Sugars and Synthesis Gas*, Office of the Biomass Program, US Department of Energy, 2004.
159 J. Wang, S. Jaenicke and G.-K. Chuah, *RSC Adv.*, 2014, **4**, 13481.
160 Y. Kuwahara, W. Kaburagi and T. Fujitani, *Bull. Chem. Soc. Jpn*, 2014, **87**, 1252.
161 X. Tang, L. Hu, Y. Sun, G. Zhao, W. Hao and L. Lin, *RSC Adv.*, 2013, **3**, 10277.

View Article Online
DOI: 10.1039/C6CY00223D

GRAPHICAL ABSTRACT

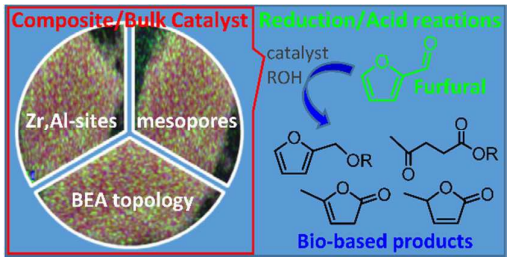

Synthesis strategies to materials integrating BEA topology, Zr,Al-sites and mesoporosity, for furfural valorization via integrated reduction/acid reactions in alcohol medium